NTNU – Trondheim
Norwegian University of
Science and Technology

Modeling of Fatigue from Random Corrosion Pits

Fredrik Øgård Sirevaag

Mechanical Engineering
Submission date: June 2015
Supervisor: Gunnar Härkegård, IPM

Norwegian University of Science and Technology
Department of Engineering Design and Materials

THE NORWEGIAN UNIVERSITY
OF SCIENCE AND TECHNOLOGY
DEPARTMENT OF ENGINEERING DESIGN
AND MATERIALS

MASTER THESIS SPRING 2015
FOR
STUD.TECHN. FREDRIK ØGÅRD SIREVAAG

Modelling of fatigue from random corrosion pits

Modellering av utmatting fra tilfeldig fordelte korrosjonsgroper

Fatigue damage related to corrosion pits has frequently been observed in aging aircraft. This has called for extensive testing and modelling of fatigue in aircraft components made from aluminium alloys. Other cases, where pitting corrosion fatigue is jeopardising the mechanical integrity of key components, are offshore pipes (including flexible risers) and blades in the region of beginning condensation of low-pressure steam turbines.

Pitting corrosion fatigue may be considered as the interaction between corrosion-pit and fatigue-crack nucleation and growth. The present work focusses on the quantitative assessment of fatigue crack growth from corrosion pits and the associated fatigue life. The number of corrosion pits as well as their size and position are assumed to be randomly distributed. Representative fatigue data for pitted specimens are compared with life predictions based on fatigue-crack growth analyses.

Tentative tasks:

- Literature search for experimental investigations and theoretical modelling of pitting corrosion fatigue of engineering materials and structures, in particular experimental data regarding
  - the size distribution and area density of corrosion pits,
  - the size and position of the critical pit and
  - the fatigue life.
- Development of a 'manual' tool for the analysis of fatigue-crack growth from corrosion pits.
- Verification of the Random-Defect module of the fatigue post-processor LINKpfat based on manual life predictions for simple components.
- Comparison between fatigue test data for pitted specimens and life predictions (mainly based on LINKpfat calculations).
- Should time permit, it would be of interest to extend the investigation to comprise a quantitative description of the growth rate of corrosion pits and its interaction with fatigue-crack growth.

Formal requirements:

Three weeks after start of the thesis work, an A3 sheet illustrating the work is to be handed in. A template for this presentation is available on the IPM's web site under the menu "Masteroppgave" (http://www.ntnu.no/ipm/masteroppgave). This sheet should be updated one week before the master's thesis is submitted.

Risk assessment of experimental activities shall always be performed. Experimental work defined in the problem description shall be planned and risk assessed up-front and within 3 weeks after receiving the problem text. Any specific experimental activities, which are not properly covered by the general risk assessment, shall be particularly assessed before performing the experimental work. Risk assessments should be signed by the supervisor, and copies shall be included in the appendix of the thesis.

The thesis should include the signed problem text, and be written as a research report with summary both in English and Norwegian, conclusion, literature references, table of contents, etc. During preparation of the text, the candidate should make efforts to create a well-arranged and well-written report. To ease the evaluation of the thesis, it is important to cross-reference text, tables and figures. For evaluation of the work, a thorough discussion of results is appreciated.

The thesis shall be submitted electronically via DAIM, NTNU's system for Digital Archiving and Submission of Master's theses.

Contact persons are:
Philippe Mainçon and Vidar Osen, SINTEF Materials & Chemistry

Torgeir Welo
Head of Division

Gunnar Härkegård
Professor/Supervisor

NTNU
Norges teknisk-naturvitenskapelige universitet
Institutt for produktutvikling og materialer

Preface

This report is a result of the work carried out as part of the master thesis "Modelling of Fatigue from Random Corrosion Pits" at the *Department of Engineering Design and Materials, Norwegian University of Science and Technology* (NTNU). The thesis continues the work that began with the project task "Fatigue Assessment of Mechanical Components with Random Surface Defects" during the fall of 2014. Chapter 1 and 2 include information gathered during the project work in the fall, but has more or less been completely rewritten as my understanding of the topic has grown. As a final task to be completed at NTNU, the field of fatigue was chosen. Being able to study fatigue over a longer period of time has proved to be both challenging and educational in terms of the technical knowledge gained, but also on a personal level of how I can work more efficiently when approaching such a daunting task.

I would like to extend my gratitude to my supervisor Gunnar Härkegård at IPM, NTNU for providing me with an interesting assignment to work on and providing valuable insights and critique on my work throughout the semester. Having him as my supervisor has helped and pushed me to create a thesis I feel proud of.

Vidar Osen of SINTEF Materials and Chemistry, Trondheim also deserves special thanks for his quick and patient assistance in using the LINKpfat software.

My parents also deserve special thanks for their relentless support during the thesis work. Their feedback during several iterations of the final report have aided me in creating a better product than would be possible without them.

Fredrik Øgård Sirevaag

Trondheim, June 10th, 2015

Abstract

This master thesis is a continuation of the project work "Fatigue Assessment of Mechanical Components with Random Surface Defects" written during the fall of 2015. Central tasks of this report has been to create a manual calculation method for the case of corrosion pitting fatigue to verify the LINKpfat FEM post-processor. Simple components subjected to corrosion pits and alternating loading have been used to validate the Random Defect module of LINKpfat. This module allows the user to define an area on a 3D component from Abaqus that will be attacked by surface defects. These defects can be defined to be randomly allocated on the surface, and their size and number can be controlled by several probability distributions. It is assumed that the corrosion pits were already established on the components and would not grow further from the corrosive environment.

A literature review was made to find the necessary data to test LINKpfat against fatigue test results. While there are many papers published on the subject it was very difficult to find all the necessary inputs well defined. Corrosion pit shape is also dependent on the material and corrosive environment. Only one fatigue test had all input parameters readily available and was used as a test on how well the software could predict cycles to failure with realistic corrosion properties. Some simplifications had to be made on the 3D component due to a weakness in LINKpfat's geometric calculation method.

Results from the fatigue test was good, considering all the variable input parameters that play a role in determining the cycles to failure. For the crack growth curve that gave the best results, LINKpfat returned conservative results that estimated roughly half the fatigue life compared to the test data. Most of the critical pits found in the software were within the expected variance due to the probabilistic distribution properties. A few statistical outliers were generated and their results seem unrealistic when compared to the average values found. This is most likely caused by some oddity in the way the generated defects are calculated when finding the critical one for each component. More validation work needs to be performed on the software side to determine why these results occur on rare occasions.

Sammendrag

Denne masteroppgaven er en kontinuasjon av prosjektarbeidet «Fatigue Assessment of Mechanical Components with Random Surface Defects» som ble skrevet i løpet av høsten 2015. Sentrale oppgaver i denne oppgaven har vært å lage en manuell utregningsmetode for korrosjonsgrop materialutmatting for å verifisere FEM postprosessoren LINKpfat. Enkle komponenter utsatt for korrosjonsgroper og alternerende last har blitt brukt for å validere Random Defekt modulen i LINKpfat. Denne modulen tillater brukeren å definere et område på en 3D modell fra Abaqus som vil bli angrepet av overflatedefekter. Disse defektene kan tilfeldig allokeres på overflaten, og deres størrelse og antall kan kontrolleres av et utvalg sannsynlighetsfordelinger. Korrosjonsgropene antas å allerede ha blitt etablert på komponentene og vil ikke vokse videre på grunn av det korrosive miljøet.

Et litteratursøk ble gjort for å finne de nødvendige dataene man trenger for å teste LINKpfat opp mot utmattingsforsøk. Selv om det eksisterer mange publiserte rapporter om temaet var det utfordrende å finne alle de nødvendige parameterne som er nødvendig for å definere alle nødvendige inndata. Bare én utmattingstest hadde alle de nødvendige data lett tilgjengelig, og ble dermed brukt som en test for hvor godt programvaren kunne anslå hvor mange sykler til utmatting et reelt tilfelle med korrosjonsgroper. Noen forenklinger ble gjort på Abaqus modellen på grunn av en svakhet i hvordan LINKpfat håndterer hull i geometrien.

Resultatene fra utmattingsberegningen var god, når man tar hensyn til alle de varierende inndataene som spiller en rolle i å bestemme utmattingslevetiden. For sprekkvekstkurven som ga de beste resultatene returnerte LINKpfat konservative resultater som estimerte rundt halvparten av utmattingslevetiden i forhold til test dataene. De fleste kritiske korrosjonsgropene som ble funnet av programvaren var innenfor de forventede variansen som skyldtes de probabilistisk fordelte egenskapene. Noen få statistiske avvik ble anslått som kritiske, men deres resultater virker urealistiske når man sammenligner de med de gjennomsnittlige resultatene. Dette skyldes mest sannsynlig av noe feil i måten de genererte defektene analyseres på når den kritiske skal finnes for hver enkelt komponent. Mer valideringsarbeid på programvaresiden bør gjøres for å finne ut hvorfor disse resultatene har oppstått noen få ganger.

Nomenclature

A	area
a	pit/crack depth
a_i	initial pit/crack depth
a_f	final pit/crack depth
c	half the length of the surface crack
C	Paris crack growth coefficient
CDF	cumulative distribution function
da/dn	cyclic crack growth rate
di	initial diameter
E	Young's modulus
erf	error function
F	geometry factor
FEM	finite element method
in	inch
ksi	kilopound per square inch
K	stress intensity factor
K_{Ic}	critical fracture toughness
ΔK	stress intensity factor range
ΔK_{th}	threshold stress intensity factor range
M_b	bending moment
N	size of sample
N_f	cycles to failure
PDF	probability density function
PDM	probability mass function
R	relationship between max. and min. stress
r	radius
s	standard deviation
U	uniform random number
v	Poisson ratio
z_0	defect density
σ_a	stress amplitude
σ_m	mean stress
λ	expected value
μ	location parameter
σ	scale parameter
σ_{ys}	yield strength
σ_{UTS}	ultimate tensile strength
α	Weibull shape parameter
β	Weibull scale parameter
θ	degree of angle

Table of Content

1. Introduction

1.1 Background

Fatigue damage related to corrosion pits can be observed in components in a wide variety of industries. In the aviation sector, this has called for substantial testing and modelling of fatigue damage in aluminium aircraft components. Corrosion pits have been found to cause serious crack growth in components with supposedly infinite life [1]. Other examples of pitting corrosion putting the mechanical integrity of critical components are offshore pipes (including flexible risers) and low-pressure steam turbine blades located in the region of beginning condensation.

Pitting corrosion fatigue can be considered as the interaction between corrosion-pit and fatigue-crack nucleation and growth. The main part of this thesis is focused on quantitatively assessing the fatigue crack growth initiating from corrosion pits and the associated fatigue life. A manual tool for considering this crack growth is developed and compared to results from the standalone FEM post-processor LINKpfat. In both these cases the number of corrosion pits and their location and size are assumed to be randomly distributed. A number of statistical probability distributions are discussed and proposed for use with corrosion pitting.

1.2 Limitation of Investigation

The thesis focuses on the investigation of corrosion pitting fatigue analysis that can be compared to the LINKpfat FEM post-processor. Tentative project tasks included investigations into the quantitative description of corrosion pit nucleation, growth and subsequent interaction with fatigue crack growth. Due to time constraints, this task was not done and the fatigue analysis assumes crack growth from already established corrosion pits.

1.3 Literature Search

During the information gathering phase of this project a variety of search engines were used. The primary search engines were BIBSYS Ask, Google Scholar and scientific databases such as ScienceDirect and Engineering Village. Some searches were also made into the archives of specific research journals such as International Journal of Fatigue. The search included various combinations of the words; fatigue, corrosion, pits, probabilistic, probability of failure, random,

surface defects, modelling, defect size distribution and crack growth. Results were evaluated by reading abstracts, and sorted by perceived trustworthiness. Peer reviewed articles was given attention, and in some cases the number of citations.

2. Theory

A summary of relevant theory reviewed for pitting corrosion and fatigue design is given in this chapter. This chapter is meant to provide the necessary the theoretical basis for making decisions when making a manual tool to best capture corrosion pitting fatigue growth. A basic understanding of fatigue and corrosion is assumed.

2.1 Fatigue crack growth and its interaction with corrosion pitting

This section examines how corrosion pits affect the fatigue life of a structure. ASTM E1823-13 defines fatigue life as "the number of cycles of a specified character that a given specimen sustains before failure of a specified nature occurs" [2]. A cycle is in this case defined as the alternating loading conditions the specimen is subjected to. These conditions can cause crack growth in the material due to the microscopic physical damage caused by each cycle above the fatigue threshold. Each successive loading cycle causes the cracks to grow, resulting in what is called *fatigue crack growth*. When the damage has reached a certain level the crack will have grown to a size that will lead to final failure for the component under the given conditions [3].

To be able to calculate the number of cycles before final failure, the process of fatigue crack growth is divided into several parts that can be assessed by various methods. One way to do this is to divide the process into two main stages, a period of crack initiation and a period of crack growth [4]. The crack initiation period is often described by crack nucleation that starts as micro-cracks at slip bands in the material. This growth is influenced by the grain boundaries and is generally not detectable until it reaches a certain size. The micro-cracks then propagate in a short-crack growth phase. When the crack has grown to a certain size, the continuing crack growth can be described by a fracture mechanical approach and is often called the long-crack phase. This continues until the crack reaches a size that makes the structure unable to withstand the given load and thus enters a failure state. The different phases are shown in Figure 1.

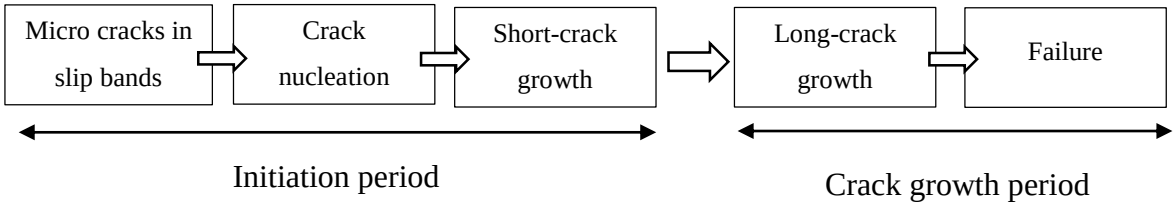

Figure 1: The two main periods of fatigue life and their underlying processes. Figure inspired by [4], but with some modifications.

Corrosion damage is a separate source of material degradation that is caused by the material having a chemical reaction with its environment. However, it too can cause crack-like discontinuities on the component surface, in the form of corrosion pits. This damage type is caused by a hostile chemical environment on the component, and can be explained as electrochemical oxidation of the metal [5]. E*nvironmental crack growth*, such as corrosion, can occur under both steady loads as well as cyclic loading, particularly if the cycling is slow or halted by time spans of steady load [3]. A further discussion of the causes and growth mechanics of corrosion pits is not given here because the thesis will consider use of a probabilistic approach to consider the pit size and density.

Pitting is a form of localized corrosion that leads to loss of material. This damage to the material can take numerous shapes depending on the material type and the environmental conditions. Pit nucleation and growth can occur by itself in a corrosive environment, but can also be aided by cyclic loading [6]. Cyclic loading can, accelerate the growth of pitting corrosion, and the fatigue crack growth can be accelerated by the corrosive environment [7] [8]. The reason for this is the protective film at the crack, or pit tip, is broken by the applied stress [9]. For this reason it can be difficult to distinguish where one failure mode ends and the other one starts. To simplify, the pit growth phase can be said to "replace" the fatigue crack growth stages shown under the *initiation period* in Figure 1. Below, in Figure 2, the process of corrosion pitting fatigue is shown. The crack initiation period is now caused by the growth of pits instead of growth from micro-cracks. Pit growth transitions into fracture mechanical cracks when they have reached a critical size.

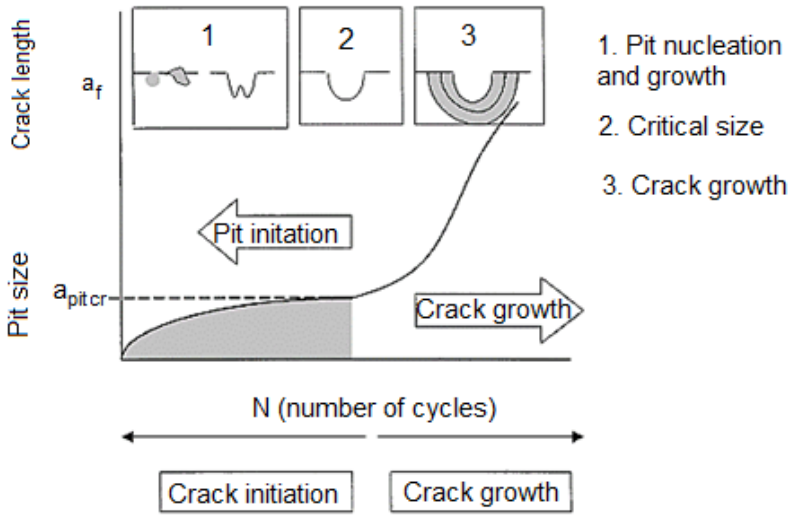

Figure 2: Initiation and propagation of fatigue crack from corrosion pit, modified from *[10]*.

For applications such as aircrafts, conditions for corrosion pit growth and fatigue crack growth generally does not exist simultaneously [11]. Cyclic loading affecting fatigue occurs when the aircraft is in flight where the temperature is relatively low and the chemical corrosion processes, which are thermally activated, will not occur effectively. Low-pressure steam turbines on the other hand experiences both a corrosive environment and operating conditions that lead to fatigue damage simultaneously. For the work with the manual tool and LINKpfat, similar conditions to the first example will be used as it allows some degree of simplification. Corrosion pits will in this approach act as pre-existing flaws from which fatigue cracks can propagate.

Corrosion pitted specimens have significantly reduced fatigue life compared to uncorroded specimens. The reduction will vary with material, loading and pitting severity. Two investigations of different aluminium alloys reported a reduction in fatigue life of 40-50 % [11] while the other reported a decrease by a factor of about 6 to 8 [12]. The main reason for the reduction in fatigue life was due to fatigue cracks initiating at the corrosion pit instead of having been subject to the initiation mechanics shown in Figure 1. To explain why the corrosion pits often act as fatigue crack initiation sites, the most cited reason is that the pits cause geometrical discontinuities on the components surface that leads to increased local stresses near the pit tip, much like conventional notches in fatigue testing [13] [14] [15].

3. LINKpfat

This chapter introduces the finite element (FEM) post-processor LINKpfat's Random Defect Module (RDA). The thesis assignment states that a manual 'tool' for the analysis of fatigue-crack growth from corrosion pits shall developed and used to validate the RDA-module. Knowledge of how the post-processor can be applied to corrosion pitting fatigue and what limitations it might have, must be understood before developing a tool that can be used to validate it. Theory presented herein derive from a paper from Wormsen et al. [16], the LINKpfat User Manual and discussions with Vidar Osen of SINTEF Materials and Chemistry, Trondheim.

3.1 Introduction to LINKpfat's Random Defect module

LINKpfat is an FEM post-processor that can do four types of analysis. Two of them, *Single Defect* and *Local Stress* are deterministic, while the two others, *Weakest Link* and *Random Defect* are probabilistic. Considering the material properties as deterministic designates them as predetermined quantities, considering them as probabilistic assumes them to be randomly distributed according to a probability distribution of some kind [16]. In the following work, the *Random Defect* module will be investigated for use on corrosion pitting fatigue problems.

The post-processor uses input from an FEM software such as Abaqus or ANSYS. An input file from the FEM software is used to generate a 3D model with an appropriate static loading case for the component that is to be analysed. Results are imported to LINKpfat from the chosen FEM software and contain the element topology, nodal coordinates and nodal coordinate stresses. The post-processor can then use the stress conditions from the input file to generate the mean- and amplitude stress that the component will have in each node. Finally, the 3D component is used to generate defects on the surface or inside the volume of the component.

Certain restrictions apply as to what LINKpfat can utilize from the input file. The load can only be considered as proportional, relative to the stress field in the FEM program. Mechanical properties will be considered as homogeneous. For the RDA module, four element types are supported: eight and twenty node brick elements as well as four and ten node tetrahedron elements. In ABAQUS the notation for these are respectively C3D8, C3D20, C3D4 and C3D10. Another restriction is the crack growth plane, which will be kept fixed as the crack grows.

Following the stress analysis in the FEM program, the corrosion pitting problem can be defined in LINKpfat [16]. The post-processor has input parameters for crack-growth rate and parameters for the probability distribution of both the number of defects and their size. In the case of corrosion pits, the defects are assigned a random location on the surface geometry by a uniform distribution. In the version of LINKpfat available at the start of the master thesis (ver. 1.2.0.3) the defects will be generated on the entire surface area of the component. In newer versions created to help with this thesis (version 1.2.0.4 and beyond, April 2015) areas free of corrosion pits can be specified. This is done by specifying the nodes that will be free of surface defects as a set in Abaqus and editing the input file (.inp) to specify the nodes that LINKpfat will ignore. As mentioned previously, the RDA module also allows for defects in the volume of the component, or both types simultaneously. Theoretically, it would be possible to investigate if corrosion pits or volume defects, like inclusions, are the most critical. In this work the focus is solely on the corrosion pits.

Crack growth is described by a Paris Law curve for the material in question and can be adjusted by inputting parameters for the Walker equation to fit the loading conditions that will be evaluated. A fatigue life calculation is done for the initial increment of crack-growth and evaluated to find the fastest growing defect, which will be considered the critical one. The full calculation for this defect is the fatigue life for the component. A Monte Carlo simulation can be performed by calculating the fatigue life for the given component several times with a new set of defects generated for each round. A set of fatigue lives for several nominally equal components are thus found and can be used to generate the fatigue life distribution for the fatigue case that have been examined.

3.2 More on RDA calculation inputs

The post-processor uses probabilistic data to generate the number of defects and their size, for the component that is going to be analysed. Theoretical basis for the concepts presented below will be more thoroughly discussed in Chapter 4, because this section is meant to provide a basis for developing the model and not explain the theory that is applied. The number of defects are determined by inputting the expected defect density, or in this case pitting density, of the area that is attacked. A Poisson distribution for this density is used to draw the number of defects that will be generated for each fatigue calculation. Number of *defects per surface area* or *defects per volume* is the only data needed to fully define how many defects should be generated.

The size of the defects, or corrosion pits, can be defined by several extreme value distributions. LINKpfat has implemented the Pareto, Normal, Lognormal, Exponential and Extreme Value distributions as possible methods to describe the size variation. Each defect distribution only allows for the initial defect to be considered as a centered half-circle, for the surface defect case, which gives the corresponding aspect ratio of a/c=1. Aspect ratio is the ratio of depth *a*, over half the surface length *c*, which can be seen in Figure 5 in the next chapter. Thus, the size distributions describe the defect radii of the corrosion pits. Only having one parameter to describe the corrosion pit might lead to some difficulties because the corrosion pit shape does not always correspond to a perfect hemisphere, see Section 4.1.1. Finding the pit metric that is most influential on fatigue life is needed, whether it is the width, depth or another measurement. Having five different distributions can be useful when investigating which one best represents the measured data. It should also be worth checking if there exists a probability distribution that is often used for corrosion pit data that is currently not implemented in LINKpfat. The size distributions can be truncated at desired maximum and minimum values if desired. When all input parameters are fully defined LINKpfat allows for repeated calculations with the same input parameters. Each iteration will generate defects with the defined characteristics, and the critical defects will be considered for each calculation.

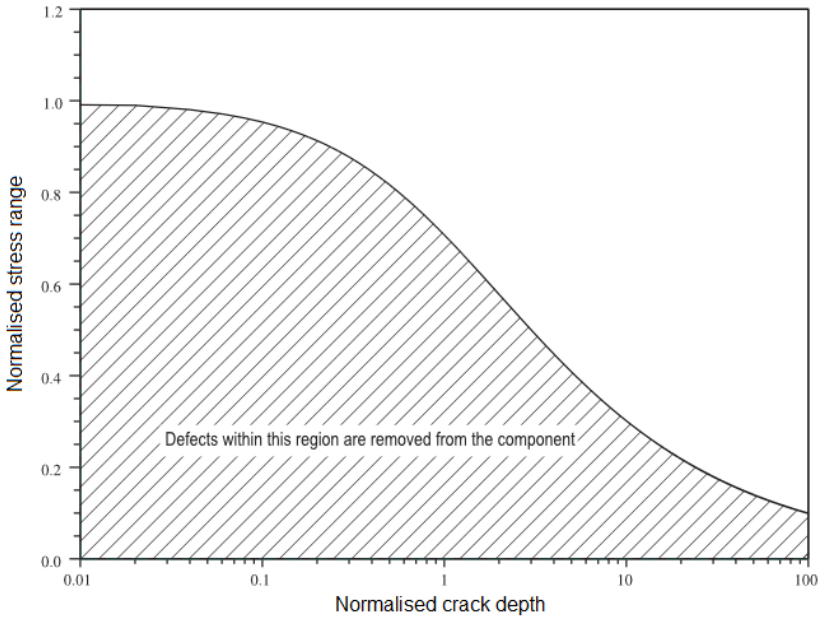

Figure 3: Katigawa-Takahashi diagram showing the discarded defects from the LINKpfat RDA-calculations [17].

The critical defects are determined by checking the generated defects versus the Kitagawa-Takahashi diagram, if a threshold stress intensity is given as input, see Figure 3. This diagram shows how the fatigue strength is affected by crack size and that there exists a critical crack size, a_{crit}, with defect sizes below this threshold considered as non-damaging. LINKpfat applies Paris crack growth law to calculate one increment of crack growth for all remaining defects. The fastest growing defect in this step will then be considered for the remainder of the fatigue calculations and the rest discarded. Using only one life-controlling defect per component minimizes calculation work when the number of defects generated are in the thousands.

The cracks are considered to grow on the plane of maximum principal stress and this plane is kept fixed as the crack grows. When the random defect module has completed the desired number of computations, it stops and provides an overview of the critical defects and their location on the component. In newer versions (1.2.0.6 and above) it is possible to also see the location of all the generated defects and not only the critical ones. Fatigue life distribution parameters are also estimated from the results in the separately completed calculations. The results of repeatedly sampling new data from the probability distributions gives information on both the worst and best possible scenarios with these loading conditions and defect distributions.

4. Model development

This chapter explains the development of the manual model developed for use with corrosion fatigue problems and for validation of the LINKpfat RDA-module. Some parts of this chapter was originally written as part of the project work in the fall of 2014, but has been reworked after feedback and a better understanding of the corrosion pitting fatigue process.

It is assumed that the corrosion pits have already been established on the surface of the component and does not grow further form electrochemical reactions. Focus has been on developing methods for generating corrosion pits on a surface, their shape and size, in a probabilistic manner. The ability to generate varied results repeatedly in a Monte Carlo fashion is important to be able to capture the inherent variance when generating data based on probability distributions. Corrosion pits will be considered as surface defects and their nucleation by electrolytic processes will not be investigated. The model was developed and implemented as a largely automated worksheet in Microsoft Excel 2013.

4.1 Corrosion pit geometry

This section presents theory about how to consider the shape of the corrosion pit in the fatigue crack growth calculations, as well as deciding upon a pit metric that can be used to define it.

4.1.1 Pit shape and crack initiation location

As mentioned in the previous chapter there are several configurations a corrosion pit can grow into. Figure 4 visualizes the shapes that needs to be taken into account by the geometric figure chosen for the simple calculation tool. The pits can be both narrow and wide, which might make it hard to find a simplified geometry that can properly address all shapes simultaneously. When considering the fatigue crack growth on the plane perpendicular to the applied stress, the right column in the figure shows the possible pit geometries that needs to be considered.

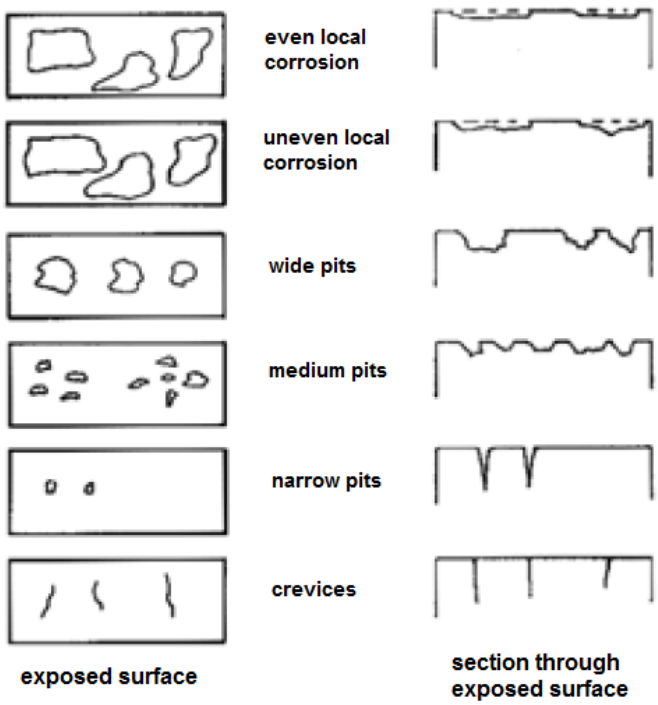

Figure 4: Types of pitting corrosion [18].

In the literature, the most commonly occurring shapes used to describe the corrosion pits are semi-elliptical surface cracks [11] [19] [20], semi-circular surface cracks [18] [21] [22] and the special case of corner cracks [21]. Härkegård also shows the two configurations in a paper, discussing these shapes for corrosion pitting application [23]. Some corrosion pit fatigue tests under laboratory conditions suggest that during initial phases the pits have a semi-circular shape, but under loading grow into a more semi-elliptical shape [20]. This was also found to occur during numerical calculations of pit development [24]. An elliptical approach could give benefits as one would be able to generate a wider variety of pit shapes. Choosing to use a semi-circular representation of corrosion pits helps simplify the calculation problem because only one parameter needs to be defined to fully describe the pit size and shape. When taking a probabilistic approach it would in the elliptical case be necessary to have data available for size distribution for both width and depth. Generating a corrosion pit from two randomly assigned values from these distributions might not automatically create a pit with a realistic combination of these two parameters. Another consideration is the fact that LINKpfat's RDA-module only allows for one input metric and defines the initial defect as a centered half-circle with the corresponding aspect ratio of a/c=1. The aspect ratio is the ratio of depth *a*, over half the surface length *c*, see Figure 5.

A semi-circle geometry as the model's defect geometry is chosen because it gives the best opportunity of comparison with LINKpfat and is a common pit geometry observed on certain materials. It is of course worth mentioning again that for some materials and corrosive environments the observed shapes may differ greatly from the one chosen here and might cause inaccuracies when predicting crack growth.

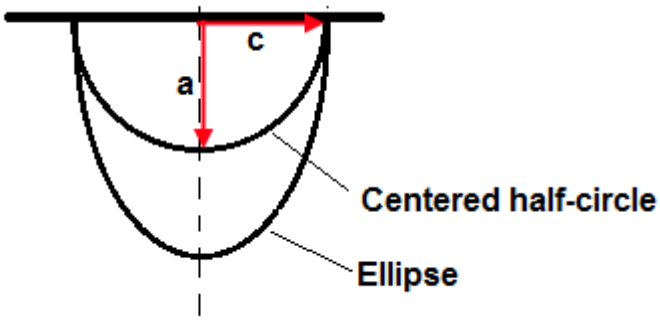

Figure 5: Illustration of two possible pit geometries and the difference in aspect ratio.

4.2 Pit metric

In Figure 6 two possible pit geometries are shown. They highlight the difference in possible pit configurations and the various measurements that can be used to describe them. According to Crawford et al [25], the most commonly used pit metrics used in the literature are depth, width and cross-sectional area. Pit depth was the most utilized by a fair margin. A pit metric is a measurable pit morphology parameter. In addition to these metrics, pit aspect ratio, pit tip radius and pit opening width are sometimes used to characterize the pit geometry.

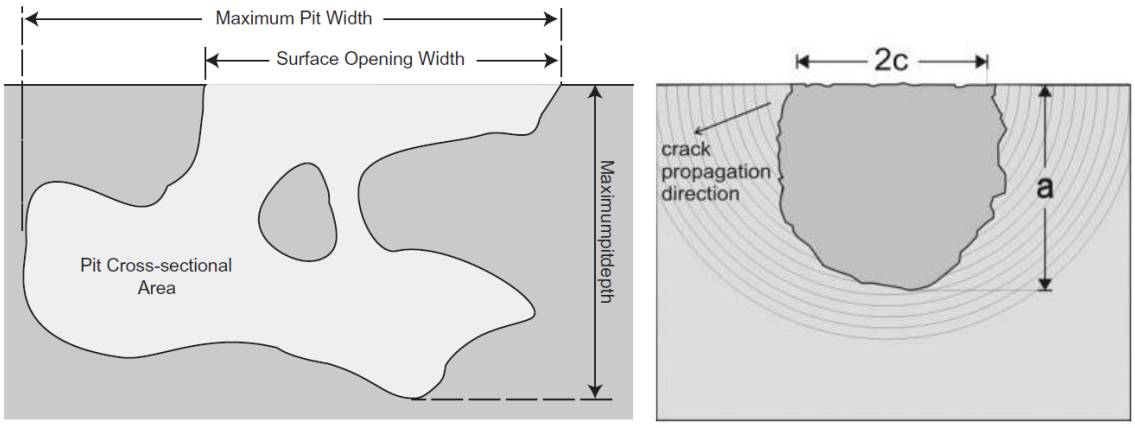

Figure 6: Illustration of different pit geometries found in the literature and associated pit size metrics. The left [1] and right [26] figure shows the variation of reported pit geometry used in the literature.

In the previous section, it was decided to only use one parameter to describe the pits. Of the metrics mentioned above the pit depth is the most relevant for this case when considering pits that are close to hemispherical in shape, such as the rightmost crack in Figure 6. For pit geometries similar to the one on the left, it could be possible to take another approach and possibly calculate an equivalent radius that a corresponding crack geometry could have if its shape had been simpler. For this manual model pit depth is used and assumed reasonably good for pit shapes that have a hemispherical shape.

4.3 Number of pits on a component

This chapter introduces a method that can be used to calculate the probability of finding a given number of defects on the surface of a component. The method is based on the application of a discrete probability distribution function where the number of defects can be drawn based on the expected defect density.

4.3.1 Poisson distribution

The number of pits on a surface is defined as the random variable *x*. As the formation of a corrosion pit is the function of several previously discussed factors, there is a need to find a distribution that can provide the probability for all the possible values the random variable could attain under similar environmental conditions. The Poisson distribution is a discrete probability distribution that has been used for similar applications [16] [27]. It describes the probability of a certain number of events occurring during a given interval. The specified interval can be matched to several criteria such as distance, time or in this case, the area of a component. The average rate of these events occurring must be known to be able to utilize a Poisson distribution.

A discrete random variable *x* is described by a Poisson distribution if it has the discrete density [28]:

$$f(x) = p(x;\ \lambda) = \frac{e^{-\lambda}\lambda^{x}}{x!} \quad \text{for } x = 0, 1, 2 \ldots, \infty \ \text{ and } \lambda > 0 \tag{1}$$

x denotes the random number of defects, while λ is a positive real number and is the expected value of the random variable and its variance. Which can be denoted by $\lambda = E(x) = Var(x)$. In the case of random surface defects, the product of expected defect density for a component z_0,

and the component area *A* where they can occur, can be used to describe the expected value λ. Equation (1) can then be modified to:

$$f(x) = p(x;\, \lambda) = \frac{e^{-(z_0 * A)}(z_0 * A)^x}{x!} \quad \text{for } x = 0, 1, 2 \ldots \quad \text{and } (z_0 * A) > 0 \qquad (2)$$

Certain conditions have to be fulfilled for the random variable to be described by a Poisson distribution [28].

1. If $I_1, I_2, \ldots, I_n$ are non-overlapping intervals, then the number of corrosion pits in the intervals are independent.
2. The exists a constant *q* such that the probability of exactly 1 corrosion pit during an infinitesimal interval of length dt is approximately equal to $q \cdot dt$.
3. The probability that 2 or more corrosion pits will occur during an infinitesimal interval is approximately 0.

In effect, this means that the presence of a defect at a location *P* on surface area *A* neither increases nor decreases the occurrence of other defects in the vicinity, or in other parts of the component. According to Wormsen et al. [16] this requires that the number of defects that could potentially be life controlling is small. In a component with a high z_0, the probability that one could get two closely located pits could be substantial. This could have adverse effects on the fatigue life calculations because there could be crack growth interaction, for parts or the entire fatigue life, which is difficult to take into account. What one could define as "small" number of defects then needs to be considered. A possibility would be to have a defect density limit to reduce the chance of this happening, as shown below. The initial defect diameter d_i would then need to be evaluated against the defect size distribution discussed in Section 4.4.

$$z_0 < \frac{1}{(10 d_i)^2} \qquad (3)$$

While such a limit might be practical for theoretical purposes, in many cases where corrosion pits are found on a surface they can be found in close proximity or in clusters where the separate instances of the pits can be hard to discern [29]. The Poisson distribution can be used to generate the number of defects, but can in some cases probably be inaccurate depending on how pit clusters are considered when investigating the attacked surfaces to find the average pit density.

4.3.2 Example of Poisson distribution applied to pit generation

An example is provided showing the PDF and CDF for a given defect density. The values were chosen arbitrarily, but show how the Poisson distribution will be used in later calculations. The parameters used are listed in Table 1.

Table 1: Example Poisson distribution parameters

z_0 [defects/cm^2]	A [cm^2]	λ [defects]
0,01	1500	15

The probability of drawing *x* defects are given by the probability mass function (PMF) graph in Figure 7. There is a possibility of getting more than 32 defects with the input data, but the results in the figure has been truncated above this value, due to the lack of visual information given. As expected the probability of finding a given number of defects peaks around 14-15 and reduces gradually on each side.

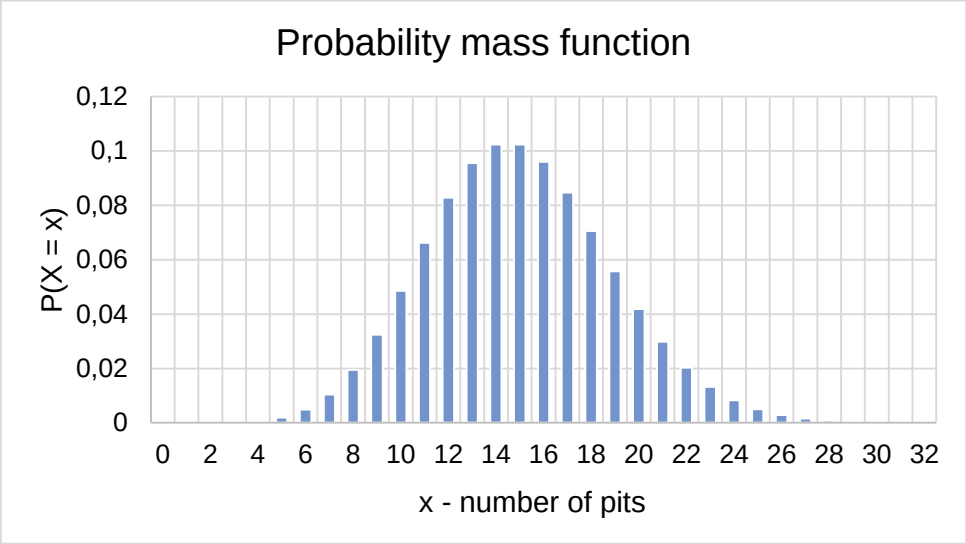

Figure 7: Probability mass function for data in Table 1.

The cumulative distribution function (CDF), Equation (4), for the discrete Poisson distribution is discontinuous due to only having a value at whole numbers. Before reaching a new integer, the ordinate value does not increase as shown in Figure 8. For each "step" between the integers the PMF value is added to the combined sum of the previous steps. The height of each step is thus the probability for that number of defects to occur.

$$F(x;\,\lambda) = \sum_{i=0}^{x} \frac{e^{-z_0 * A}(z_0 * A)^x}{i!} \quad for\ x = 0, 1, 2 \ldots \quad and\ \lambda > 0 \tag{4}$$

Below is an example on how this can be performed. Consider the uniform distribution U(0,1), which has an equal probability for all values between 0 and 1. For the sake of example consider the case where U = 0,2 has been generated. Draw a line from this value on the ordinate, in Figure 8, until it intercepts the first vertical line between the plotted points and the integer value on the abscissa. In this case the line intercepts x = 12 and this is then the number of defects generated. A visual representation of this defect generation is shown in Figure 8. The CDF values would with this method provide the threshold values for each number of defects. In the unlikely event of the U-value being exactly equal to a threshold value with several decimals, a coin-flip methodology could be applied to decide between the two integer values considered.

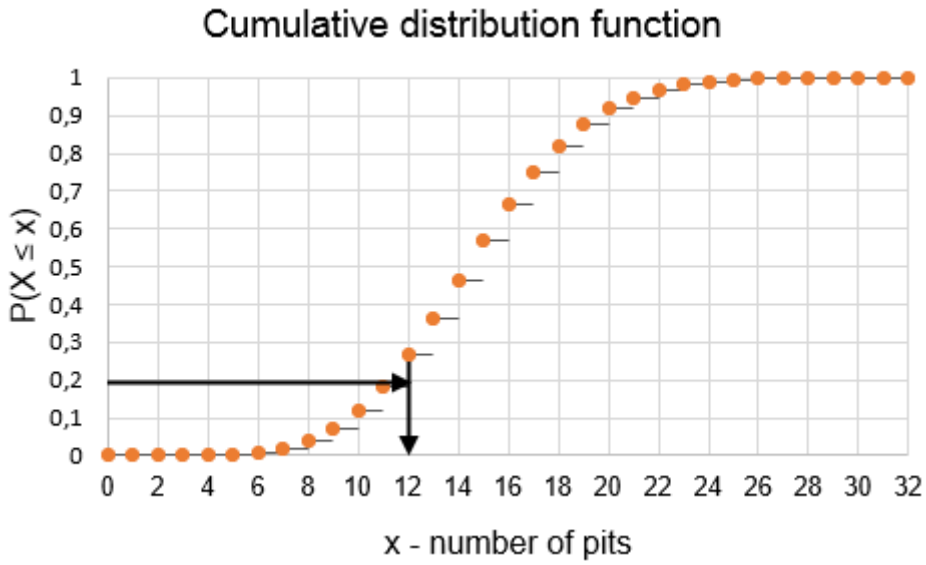

Figure 8: "Drawing" number of defects from a Poisson distribution.

4.4 Pit Size Distribution

As previously discussed, the size a corrosion pit can take depend on various factors. To be able to describe the probability of a pit adopting a given size one needs some sort of continuous probability distribution that can be determined from for example observed sizes during service or experiments. From Section 4.2, pit depth was chosen as the metric to be considered.

4.4.1 Weibull distribution

An approach considered was to fit reported pit depths in the literature to a two-parameter Weibull distribution. This is something Crawford et al. have done [30], among others. As mentioned in Chapter 3 there are several possible defect distributions available in LINKpfat.

The two-parameter Weibull is not one of them, although it is a part of the GEV, but is there inversed. To test this approach, data collected by Crawford et al. [25] was used in the calculations below. It is important to note that this data is merely the mean reported pit depth from 30 sources on aluminium alloy in the 2000 and 7000 series. Some values are from in-service conditions and some from experiments. Since the pit depth derives from many different sources, and thus environments, it is not applicable to a specific case but gives a reference to see what the expected sizes of corrosion pits will be when looking for data on the calculation cases. The data will illustrate the mean pit depths that can be expected to be observed under various environments, and the goal in this part was to learn how to determine the parameters in the extreme value distribution (EVD) and not for a specific application.

A random variable *x* is Weibull distributed if it has the probability density [28]:

$$f(x;\alpha;\beta) = \begin{cases} \alpha\beta^{-\alpha}x^{\alpha-1}e^{-(x/\beta)^{\alpha}}, & \text{if } x > 0 \\ 0, & \text{if } x < 0 \end{cases} \tag{5}$$

Linear regression was performed in Excel to find the constants α and β. This was done by integration of Equation (5) and fitting the data to a straight line. The result was a shape parameter α = 0.83 and scale parameter β = 165 µm. These values were then used to create the PDF and CDF for pit depth up to 1600 µm.

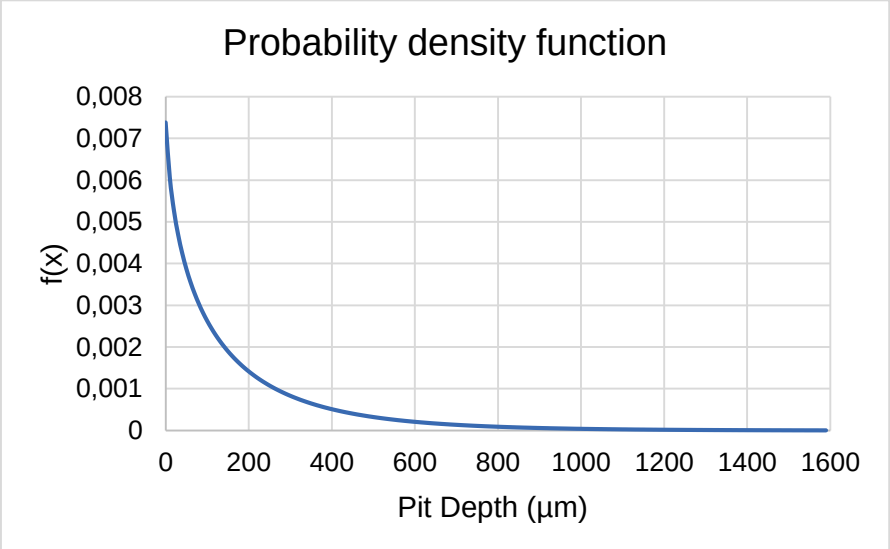

Figure 9: Probability density function of the Weibull distribution. There are possible data points above the values shown on the abscissa, but the graph was truncated at this value.

Figure 9 shows that the there is a greater probability for small pits than larger pits. This fits well to how the data was represented in a frequency histogram in the Crawford paper. The CDF shown in Figure 10 shows that the cumulative probability of getting a pit depth below 200 µm is 70 %. The CDF does not converge at a value of 1 at 1600 as could be assumed from the graphical representation, but allows for larger defect sizes. The cumulative distribution function for the two-parameter Weibull distribution is:

$$F(\mathrm{x};\alpha;\ \beta) = 1 - e^{-(x/\beta)^{\alpha}} \tag{6}$$

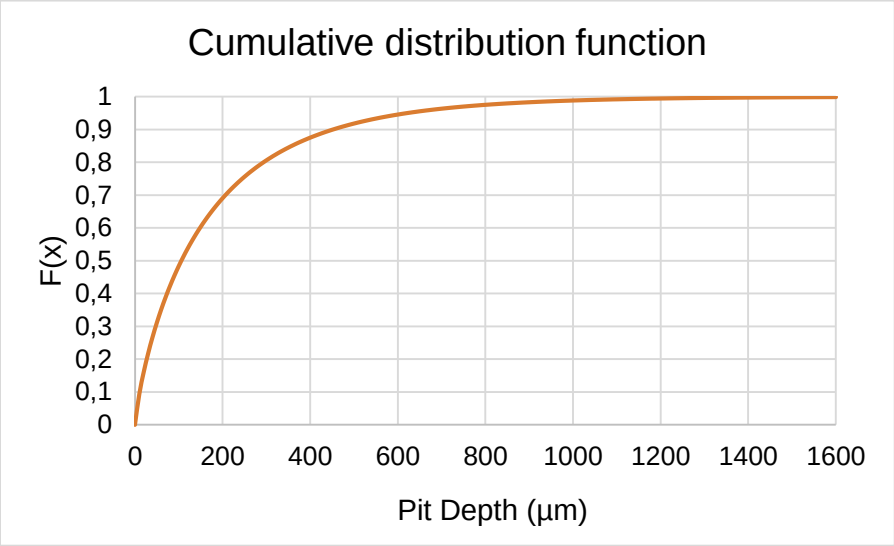

Figure 10: Cumulative distribution function of the Weibull distribution. There are possible data points above the values shown on the abscissa, but the graph was truncated at this value for visibility.

While the data seems to fit the pit depth values well, probability plotting to determine the goodness-of-fit of the Weibull distribution to these data was performed. This can be done by finding the R-squared value, which indicates how well the plotted points from the linear regression fits to a straight line [31], see Figure 35, Appendix A.3. An R-squared value of 1.0 would indicate a perfectly straight line and an optimal fit. The value found for this Weibull curve was an R-squared value of 0,97. This would indicate a quite good fit for the Weibull distribution for the data set. Determining a given defect size to be assigned to a generated pit could be done similar to the approach discussed in Section 4.3 for the number of pits. The only difference is that in this case, it would be done on a continuous distribution and one would not need to look at the value found between the incremental steps.

4.4.2 Other probability distributions and data fitting methods

Does the use of this type of continuous probability function make sense for corrosion pits even though the data itself fits well to a two-parameter Weibull distribution? Would a sample size of 30 pit depths give a realistic representation of the real pit depth population (disregarding the fact that the observed corrosion pit depths for this distribution derives from different materials and conditions)? These are rather complex questions to answer. A new data set with more data points would most likely generate a distribution characterized by slightly different constants. Whether or not this would have a large effect on the final fatigue life depends on the variance in the reported data and other factors such as stress amplitude. Another continuous probability distribution could also have been selected, and can for other data sets give a better fit with R-squared values closer to one. A method to quickly compare several probability distributions would be beneficial. One such tool that enables quick comparisons is the EasyFit software by Mathwave Technologies [32]. This tool will be used in later calculation attempts. Having many different types of probability distributions can be very beneficial because different types of distributions can best describe different sets of data. The manual approach can use any defect distribution that is deemed useful, but whereas LINKpfat is limited to five. A method to implement more defect distributions, or being able to easily write the code on how to draw other distributions could be useful. Figure 11 below, shows the general outline of each distribution type available in LINKpfat and the two-parameter Weibull distribution.

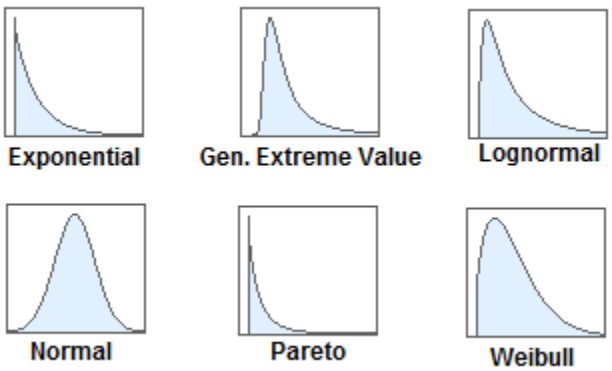

Figure 11: A simplified comparison of the general shape of the five LINKpfat probability distributions and the proposed Weibull distribution [33].

Another consideration is how the sample sizes have been measured. An approach is to only consider the largest defects by applying statistics of extremes as Wormsen et al. did for

randomly distributed volume defects [16] and Andersen et al. did for large inclusions in steel [27]. When using this method the goal is stochastically expressing the quantity of unusually large or small defects [34]. To do this the block maximum or peak-over threshold methods are cited as possibilities. Further investigations into the effects of these methods to measure pit depths are not discussed, but kept in mind when analysing the reported pit depths in the later comparison calculations.

4.5 Generating Defects on a Surface

When the size and number of defects that exists on a surface is known, there is a need to be able to distribute them on the surface of the component. This chapter discusses methods on how to generate defects randomly on a simple surface.

4.5.1 Uniform distribution

As an initial investigation, a flat surface was considered. In a 2D plane, a Cartesian coordinate system can define the defect's position. To assign a random position it would then be necessary to generate a random value for the X and Y coordinates within the boundary set by the length *L* and width *W* of the rectangle. A mathematical description of way to do this is given in Equation (7). Here U is a uniform random number between 0 and 1.

$$\begin{bmatrix} x \\ y \end{bmatrix} = \begin{bmatrix} U_1 L \\ U_2 W \end{bmatrix} \tag{7}$$

Using Equation (7) and inserting values for length and width, L = 300 mm and W = 400 mm for an example rectangle, gave the locations given in Figure 12. The figure includes two sets of randomly generated numbers between 0 and 1 to show how the location can vary for each calculation.

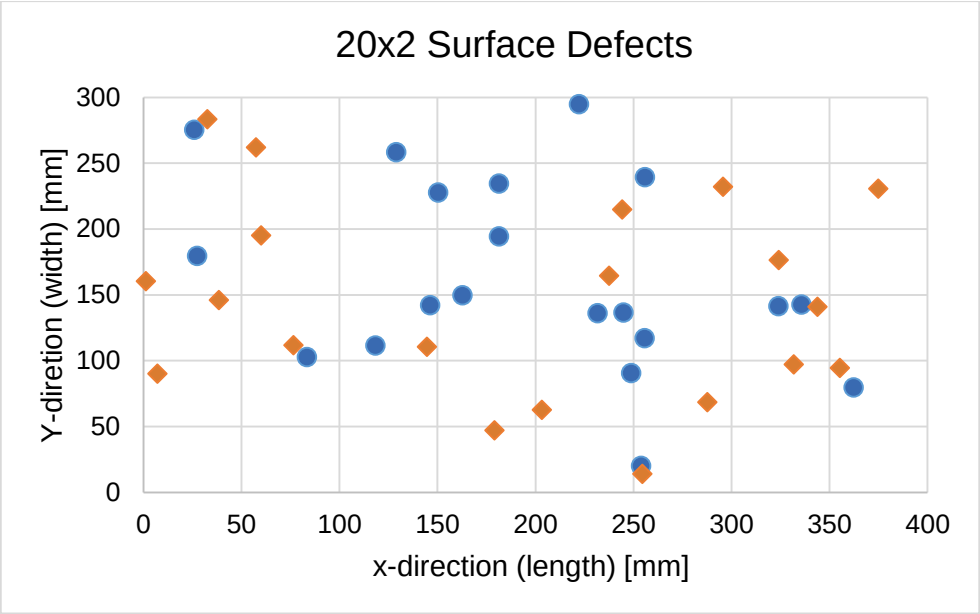

Figure 12: 20 randomly generated defects for two separate sets of ten.

There are of course some obvious limitations such as the inability to consider 2D planes with non-perpendicular edges. Pits that gets located at an edge also needs to be considered somehow. Two points at approximately (360, 120) almost looks like a single defect because they are defined at nearly the same coordinate. This could cause interaction issues in the fatigue calculations depending on the initial size of the defects. One would thus need either to make size restrictions where this method could be applied or make simplifying assumptions in regards to crack growth interaction. This method will then give the exact location of the pit and the stress for the pit can be derived for this location.

4.5.2 Surface sectioning

If the exact location is not too important and the stress situation is reasonably simple, a simplification can be made. For the case of a cantilever beam subjected to a given load at the edge, the compressive and tensile stress will be linearly distributed along the length of the beam. To calculate the stress for the exact location each pit would have on the beam could require a high number of calculations, depending on the number of pits. A simplification can be done if the beam is partitioned into sections along the length and then only calculating the mean stress within each zone for all the pits found within. The pits that are generated on each section can be sorted by size and only the largest would need to be considered for each zone.

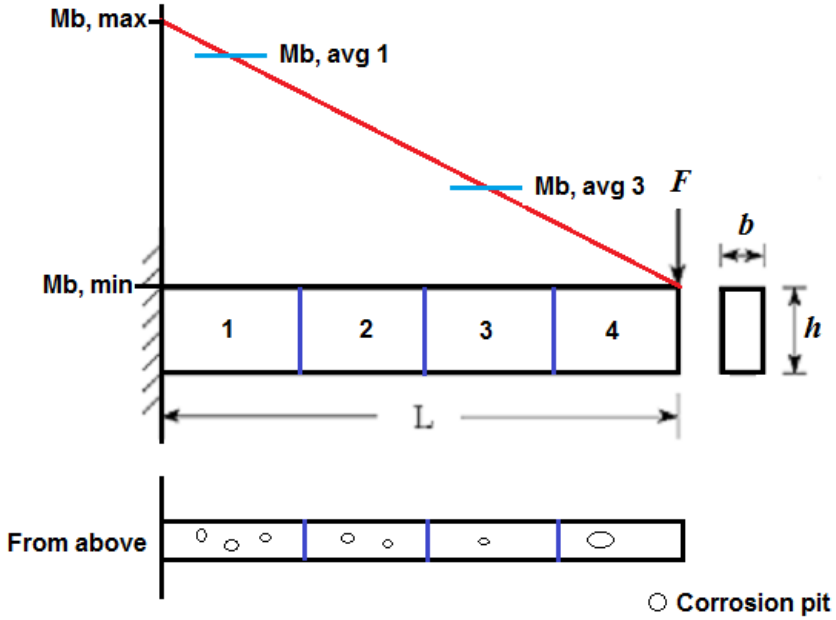

Figure 13: Sectioning of component and sorting by largest defect in each partition.

The number of partitions for the beam can easily be adjusted to find the most critical areas of the component. In the case shown above there is a high likelihood of most critical pits being in section 1 or 2, but it could be useful to have a more detailed representation of the distribution close to the fixed end. If the pits are assigned to each section randomly, the size of each section needs to be identical if the distribution is going to be uniform.

4.6 Crack growth

For the crack growth part of the model it was decided to use Paris Law for the entire crack growth length. There was no differentiation between the short- and long-crack regimes. The following equations were used and the geometrical factor F was kept constant and not recalculated of each increment.

$$\Delta K_i = F\Delta\sigma\sqrt{\pi a_i} \tag{8}$$

$$\left(\frac{da}{dn}\right)_i = C * \Delta K_i{}^m \tag{9}$$

The Paris Law in Equation (9) was reworked into Equation (10) to calculate the fatigue life for each increment. The calculations done in the project was kept to 0,5 mm steps where *ΔK* was recalculated for each increment.

$$N_i = \int_{a_{i-1}}^{a_i} \frac{1}{C}(\Delta K)^{-m} da = \frac{1}{C}(\Delta K)^{-m}(a_i - a_{i-1}) \tag{10}$$

In the project work it was discovered that such a large increment size would give a considerable calculation error compared to the LINKpfat calculations. To get an accurate step the result for Equation (10) was compared to the analytical solution for Paris Law, shown in Equation (11).

$$n(a_i, a_f) = \frac{a_i}{da/dn_i} * \frac{1 - (a_i/a_f)^{\frac{m}{2}-1}}{\frac{m}{2} - 1} \tag{11}$$

The increment steps were readjusted to 5 μm which allowed for a difference of less than one percent while keeping the number of calculation steps reasonable.

4.7 Monte Carlo Simulation

A Monte Carlo approach could be selected as a method to take into account the varying results one could get by each sampling from the probability distributions. The Monte Carlo method creates synthetic system data by repeatedly doing the calculation and as a result gives an overview of the possible outcomes experienced by the component [28]. Looking at defect generation, each repetition of the fatigue calculations in a Monte Carlo simulation will give a varying number of pits, pit depths and their location on the component. Critical pits will thus vary by the new combinations of location, size and nodal stress found for each iteration. Each input parameter would vary according to their respective probability distributions. The results can then be evaluated in for example a histogram to assess the fatigue life distribution the component can experience. Figure 14 shows a flowchart of how a Monte Carlo simulation could be configured with the defect generation methods discussed in previous chapters.

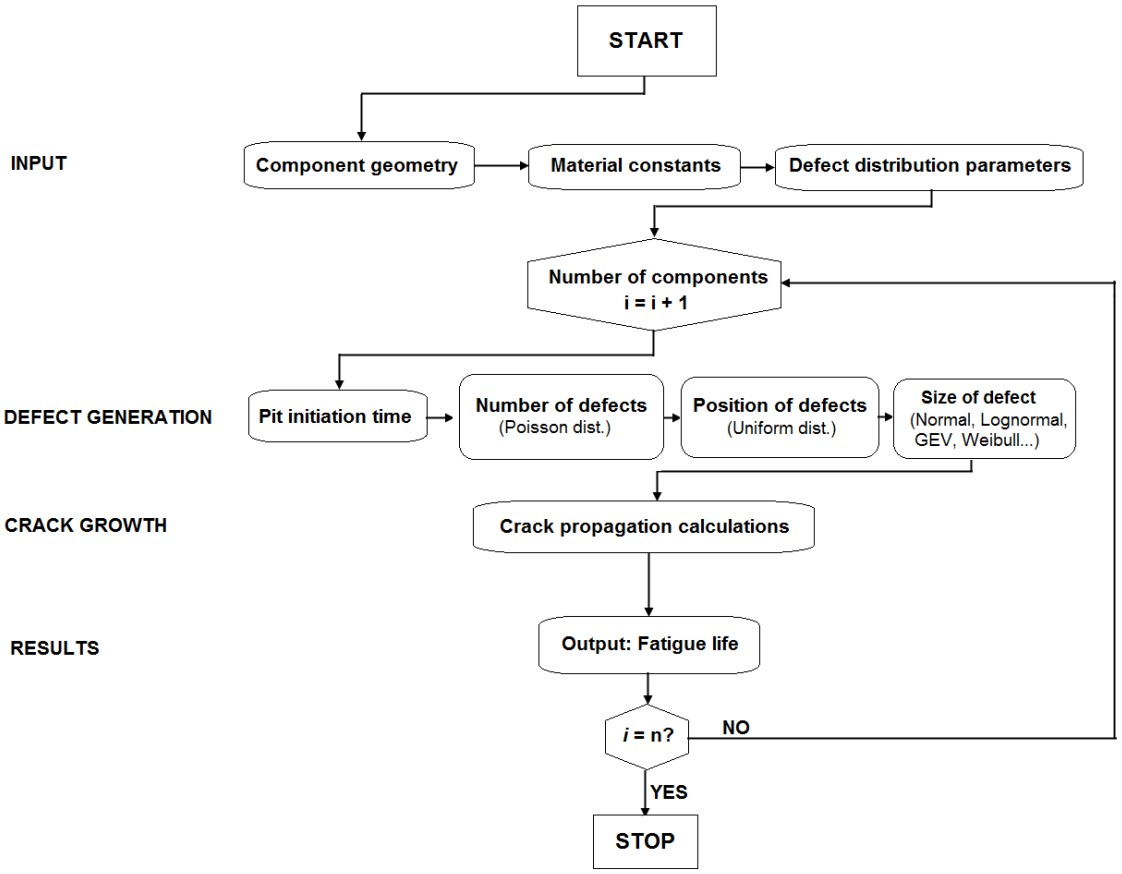

Figure 14: Schematic representation of a possible configuration of the Monte Carlo simulation of several similar components.

The figure can be divided into several main parts shown on the left side. The model shows the calculation loop required to create the synthetic system data for the investigated component. While the input parameters are static, new defect distributions will be generated for each iteration. The calculations stop when the desired number of repetitions *n* have been completed with the results from each calculation stored. After the Monte Carlo simulation has completed the results can be analysed to find trends in the system, such as standard deviation. In this version, the pit initiation time and pit growth/crack growth interactions have not been included.

5. LINKpfat compared to “manual model”

This chapter provides two calculation comparisons between the developed Excel model with the setup from Chapter 4 and the LINKpfat software described in Chapter 3. The input file for LINKpfat was modelled and given the appropriate loading conditions in Abaqus 6.13. A few extra tests on certain aspects of LINKpfat were done after each case, as needed, to verify some of the results.

5.1 Case 1: simplified turbine blade in tension loading

The first test case that was investigated was a simplified L-1 steam turbine blade with corrosion pits subjected to fatigue loads from alternating tensile (centrifugal) force. This test was originally done during the project work preceding this thesis, but it was discovered during this calculation test that the RDA module had problems generating surface defects correctly. Some surface cracks were generated, but they were facing random directions and was located in the volume of the components, and were in effect embedded cracks. A purely circular embedded crack was also created in some rarer cases. An example of this is shown in Figure 36, Appendix B.1, and compared to the correct surface defect configuration. As a result the fatigue life calculations of LINKpfat was nowhere close to the estimated values for the manual tool. There was no time to fix this before the project work was due, and the test was recalculated with a new version of LINKpfat developed in January 2015 that addresses this issue.

5.1.1 Calculation inputs

To have the possibility for comparison with the project results, the project work calculation inputs was used. Material- and other calculation parameters are shown in Table 2. The mean stress in tension is shown, but not used directly in the calculations. Mean stress usually influences the crack propagation in steels and aluminium [35], but this effect has not been included here. For the Abaqus model the mean stress was used to model after and the amplitude for the LINKpfat calculations were derived from it. Abaqus model, with mean stress, is shown in Figure 38, Appendix B.1 The fatigue life calculations in both cases stop when the crack has reached half the thickness of the blade, considered as the critical crack state. For the Monte Carlo simulation it was decided that calculating, the fatigue life a total of 10 times would be enough to show the variance the two solutions could experience. For the manual calculation, it was assumed that the uniform stress field in the component would cause the largest drawn

corrosion pit to be the critical one. In this version of LINKpfat (v.1.2.0.3) it is not possible to choose where to generate the surface defects. Corrosion pits, even in locations where you would most likely not have any, such as the top- and bottom surface, will thus attack the surface. This assumption was also applied to the manual calculations for consistency.

Table 2: Variables used to calculate corrosion pitting fatigue on simplified turbine blade in tension.

Parameter	**Value**	**Component geometry**
Blade length l [mm]	500	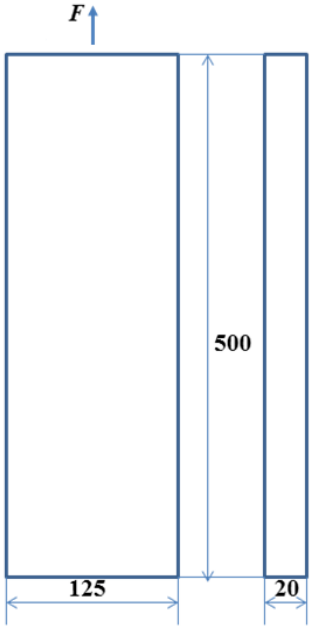
Blade width w [mm]	125	
Blade thickness t [mm]	20	
Final crack depth a_f [mm]	10	
Normal dist., scale parameter σ [µm]	87,678	
Normal dist., location parameter μ [µm]	219,63	
Defect density z_0 [pits/cm^2]	1	
Mean stress σ_m [MPa]	517,5	
Stress amplitude σ_a [MPa]	57,5	
Paris mat. constant C [(m/cycle)/(MPa m^{0,5})^m]	1,1*10^{-11}	
Paris mat. constant m	3,37	
Geometrical factor F	1,12*(2/π)	

Data for size distribution of corrosion pits was during the project work limited and was obtained from the reported mean critical pit depths from a DSTO report [36]. This is not a perfect representation of a possible corrosion pit distribution, but was used as it had sizes well within the expected bounds of Figure 9. The raw data gave the best fit for a normal distribution as seen in Figure 15.

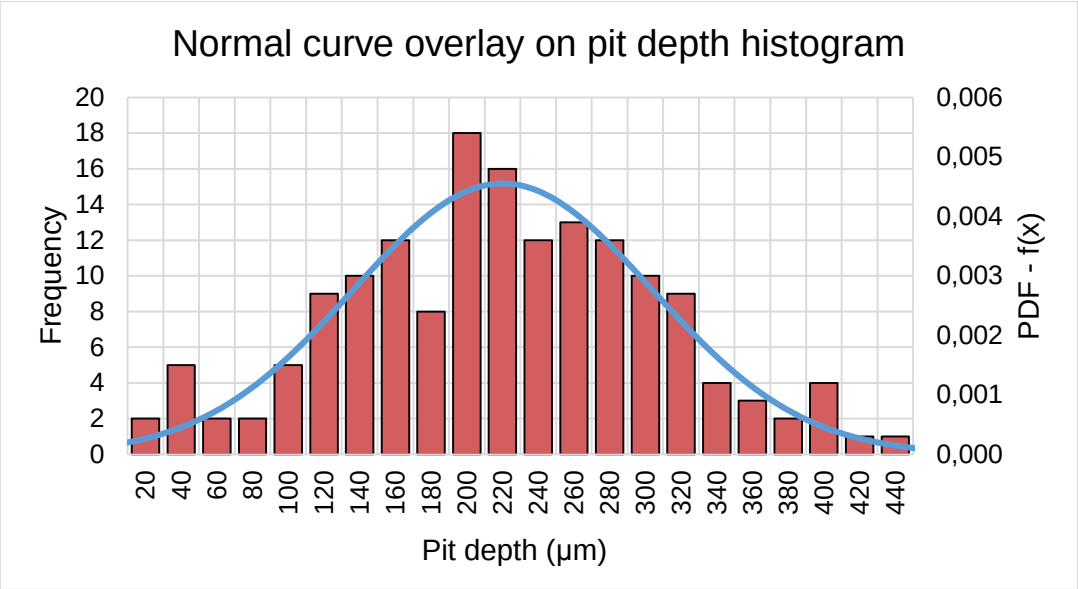

Figure 15: The best fit on the pit depth histogram was a normal distribution. The corresponding CDF curve used to draw the defect size shown in Figure 40, Appendix B.2.

5.1.2 Calculation results

Table 3 shows the results for ten components for each calculation method, sorted from lowest number of defects generated to highest. There are primarily three things that can be compared; how many defects are drawn, initial size of the critical defect, and the fatigue life. Their average value, their range and the percent relative range (PRR) can be used to compare them. The formulas for these comparison calculations are shown in Appendix A.2.

LINKpfat vs. manual calculation

Table 3: Comparison between ten components generated both manually and with LINKpfat.

	Manual calculations			**LINKpfat (v.1.2.0.3)**		
#	**Defects**	**a_i [µm]**	**N_f [cycles]**	**Defects**	**a_i [µm]**	**N_f [cycles]**
1	1464	479	$1{,}16 * 10^7$	1403	470	$1{,}27 * 10^7$
2	1465	534	$1{,}07 * 10^7$	1419	547	$1{,}16 * 10^7$
3	1468	543	$1{,}06 * 10^7$	1443	511	$1{,}19 * 10^7$
4	1505	482	$1{,}16 * 10^7$	1487	473	$1{,}30 * 10^7$
5	1507	529	$1{,}08 * 10^7$	1499	501	$1{,}21 * 10^7$
6	1515	502	$1{,}12 * 10^7$	1499	491	$1{,}23 * 10^7$
7	1518	542	$1{,}06 * 10^7$	1506	534	$1{,}15 * 10^7$
8	1522	587	$9{,}92 * 10^6$	1528	527	$1{,}16 * 10^7$
9	1529	531	$1{,}07 * 10^7$	1568	509	$1{,}19 * 10^7$
10	1552	528	$1{,}08 * 10^7$	1596	461	$1{,}29 * 10^7$
Average	1504,5	525,7	$1{,}09 * 10^7$	1494,8	502,4	$1{,}22 * 10^7$
Range	88	49	$1{,}68 * 10^7$	193	86	$1{,}42 * 10^6$
PRR	5,85 %	9,32 %	10,80 %	12,91 %	17,12 %	12,4 %

The percentage difference between the average fatigue life for the manual calculations and the LINKpfat ones are roughly 12 %. Differences is to be discussed in Section 5.1.3.

LINKpfat results, compared to analytical solution

To give a more direct method of comparison for the fatigue life calculations, the depths that LINKpfat determined as critical was used as input for the analytical solution. The results are presented in Table 4.

Table 4: Analytical calculations for LINKpfat critical defect size compared to LINKpfat fatigue lives.

#	a_i [µm]	LINKpfat, N_f	Analytical, N_f	N_{pfat}/N_{an}
1	470	$1{,}27 * 10^7$	$1{,}18 * 10^7$	1,077
2	547	$1{,}16 * 10^7$	$1{,}05 * 10^7$	1,103
3	511	$1{,}19 * 10^7$	$1{,}11 * 10^7$	1,076
4	473	$1{,}30 * 10^7$	$1{,}18 * 10^7$	1,082
5	501	$1{,}21 * 10^7$	$1{,}12 * 10^7$	1,076
6	491	$1{,}23 * 10^7$	$1{,}14 * 10^7$	1,077
7	534	$1{,}15 * 10^7$	$1{,}07 * 10^7$	1,075
8	527	$1{,}16 * 10^7$	$1{,}08 * 10^7$	1,076
9	509	$1{,}19 * 10^7$	$1{,}11 * 10^7$	1,077
10	461	$1{,}29 * 10^7$	$1{,}20 * 10^7$	1,077
Average	-	$1{,}22 * 10^7$	$1{,}12* 10^7$	~1,08
Range	-	$1{,}42 * 10^6$	$1{,}51 * 10^6$	-
PRR	-	12,4 %	11,6 %	-

These calculations show that the difference between the fatigue lives calculated by the Paris Law implementation is averagely around 8 %. This is a 4 % reduction compared the difference found in Table 3 calculated in the previous section and the difference is most likely caused by the small sample size and the critical defect size. A larger sample size would likely reduce this gap to some extent.

5.1.3 Result discussion

Defect generation and critical defect

From the results presented in Table 3 and Table 4 there are several interesting findings that can be discussed. Firstly, the number of defects drawn shows a notable difference. The average is number of pits are quite similar to the expected value of 1500. It is likely that with a larger sample size both these values would be closer to the expected mean value. It is however quite noticeable that the range for the number of defects drawn with LINKpfat is much higher than

the manual method. The PRR value is over twice as high and could be a cause for concern. This because it could have a direct impact on the likelihood that very large defects are drawn, which might be the reason that also the critical defect size has a much larger range than the manual calculations shows. It might be a stretch to assume that an error in the selection exists from the limited data, as another Monte Carlo simulation could cause the average and range of the critical defect to be different. Another cause might be the assumption that the largest defect is the critical one. LINKpfat might have found a smaller defect as the critical one from the initial crack growth rate calculations. In a component with a uniform stress field this should not occur, unless some defects are located at the edges with parts of the defect sticking outside the 3D model and not being able to assign nodal stress for the outlying parts. This should cause the software to assign the crack as a corner crack in most cases. The manual model does not take into account the specific location of each pit and assumes that all parts are within the component. Sample size could also play in here so there is a need to do additional testing on the defect generation part of the RDA module. A test performed for the Poisson distribution implementation of LINKpfat is shown in Section 5.2.

Fatigue life

From calculating the fatigue life of ten components with unique defect properties the difference between the average fatigue lives were found to be around 12 %. To control for variance caused by the sample size, the calculations for the pit depths found in LINKpfat were used as input in the analytical method. This reduced the difference by around 4 %. The PRR difference also became below 1 % between the calculation methods. Why there is a difference of 8 % between the LINKpfat calculations and the analytical one is mostly speculation. One reason might be that the simple Paris Law implementation used for the manual calculation assumes the geometry factor F to be constant as the crack grows. LINKpfat takes this the changing crack geometry into account, and as a result the a/c-ratio does not equal 1 when the final crack depth has been reached. The width of the defect has grown faster due to the re-evaluated geometry factor for each increment. Another reason is that the manual tool assumes an infinite plate, while the thickness is only twice as deep as the final crack depth. LINKpfat considers the finite thickness, and should also consider the changing of the geometry factor if the pit is located close to the edge of the component and becomes a corner crack. From Case 1 LINKpfat gives slightly conservative results compared to a simple Paris Law calculation, but might be more correct due to the ability to re-evaluate certain parameters during calculations.

5.2 Poisson distribution – mesh sensitivity check

The results for the number of defects drawn in Table 3 showed that there was a considerable difference between the results of LINKpfat and the manual model. A test was performed to check the two possible reasons for this variance. One reason could be that the sample of ten components was too low. Another was the difference in how the manual model and LINKpfat uses the Poisson distribution to draw the expected number of defects. For the manual calculations, the surface area input in Equation (4) is the total area affected by corrosion pits. In LINKpfat the area of each element is used as input, and defect number is calculated for each of the mesh elements separately. The total number of defects for the model are then summed together.

To test what the cause of the difference was, 300 components were set as the new sample size to account for the variance caused by the distribution. The number of defects was calculated for 300 units manually, and the same was done for two components with different mesh densities. To ensure that a possible mesh dependency could be observed the components mesh density was increased by a factor of 15 between them. The lowest density used was the same as the one used for the calculation in the uniform tension loading case, 2400 elements of C3D8. The model with the highest density thus had 36 000 C3D8 elements. The Abaqus model mesh comparison is shown in Figure 16.

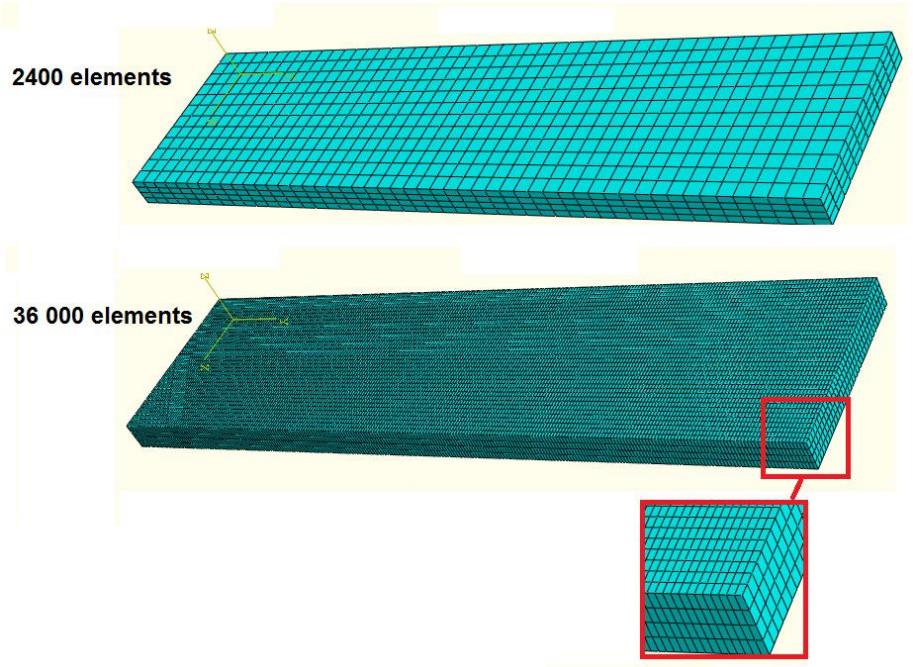

Figure 16: The different mesh densities used to check the Poisson distribution.

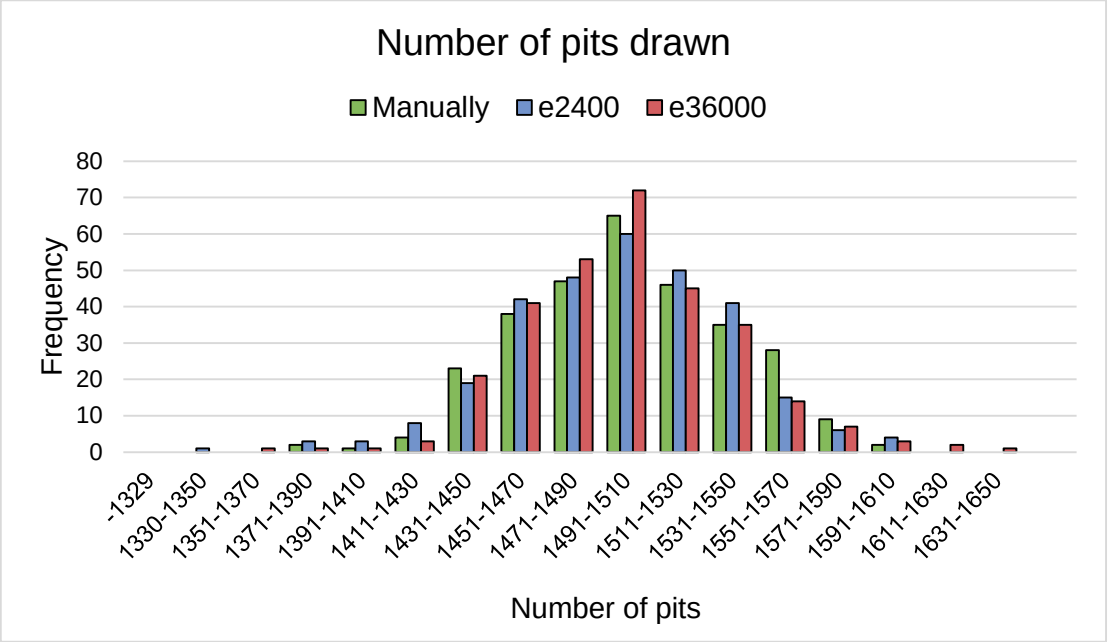

Figure 17: Number of pits drawn histogram for the three compared cases.

The histogram in Figure 17, shows the distribution of the number of drawn pits for the 300 instances of each case. No clear indication is found that the mesh density makes a large impact on the number of pits drawn. Most of the difference is probably caused by the variance and would most likely be minimized further with an even larger sample size. This was not done because there seemed to be good enough results to conclude that there was not too much of a difference. Table 5 shows some of the data for each of the cases. Each average value is as expected close to 1500 in all cases. Standard deviation results are also very close. The highest and lowest amount that are drawn are reasonably similar and are mostly outliers. How the random numbers that are used to draw from the Poisson distribution can also make an impact on the results. Excel 2013 and LINKpfat might have implemented the Random Number Generator (RNG) algorithms differently and may cause some pseudo-random numbers instead of true randomness. Such an investigation might be of interest, but is not pursued further here.

Table 5: Comparison data for the three cases.

Type	Average	Standard dev.	Highest pit count	Lowest pit count
Manually drawn	1501,10	39,2	1599	1371
2400 elements	1497,45	40,9	1608	1340
36 000 elements	1500,23	40,1	1635	1359

From the above data, it is concluded that there is not a heavy mesh density dependency on the method LINKpfat uses. It might have a slight impact on how the number of defects are distributed when drawing on *n* number of components depending on the RNG results. The small differences this causes will probably not have a large impact on the final fatigue life.

5.3 Case 2a – simplified turbine blade subjected to bending (pfat v1.2.0.9)

From the first loading case of uniform tension stress LINKpfat was found to give reasonable results for the critical defect. There was some uncertainty about whether or not the reason for the slightly smaller critical defects than for the manual solution was due to how the software chose the critical defect. As mentioned in Chapter 3 the software calculates the initial crack growth rate for each generated defect and uses the one with the highest *da/dn*. A test with the same simplified turbine blade geometry was used to evaluate how LINKpfat chooses the critical defect when the maximum stress changes linearly across the surface. By request, Vidar Osen, a developer at Sintef Materials and Chemistry, developed a method to specify the surface regions that would be attacked by corrosion pits. This enables overlooking surfaces that would most likely not have critical corrosion pits such as the sides and the fixed end. The turbine blade is in this case modelled with only the tension and compressive forces from the steam hitting the front of the blade. Corrosion pits were allocated only on the front surface, which experienced tension.

5.3.1 Calculation inputs

Manual model

The manual model was designed after the concept discussed in Section 4.5.2. It is based on an approximate location for the corrosion pits by dividing the attacked surface into equally sized sections. In the case of a linear stress, the average bending moment of the section is used for the entire section surface when calculating the fatigue life. This is an approximation that will lead to some fatigue life differences compared to LINKpfat, but will still allow for a reasonable comparison between the most common locations for the critical pit. Each section added will increase the accuracy of the predictions. Therefore, it was decided that 24 would be a reasonable number of sections. Figure 18 shows the section length and the reference numbers that will be used in the results table. However, it was assumed that the largest defect in each section would be the critical one for that section. Each section's fatigue life was calculated, and the lowest number was the critical one. Parameters used for fatigue calculations is gathered in Table 6.

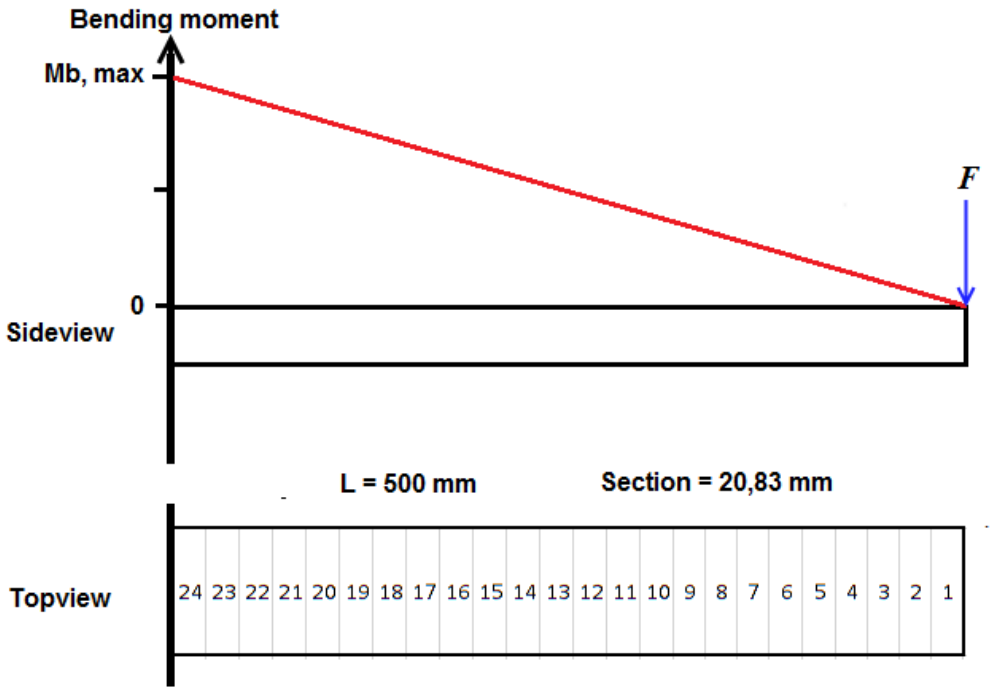

Figure 18: Load case and manually modelled sections.

The stress situation for this beam will include tension stress on the top surface, and a compressive stress on the underside. Cracks growing from the top surface towards the bottom will grow into a decreasing stress field. Paris Law and the stress intensity relation used in the previous case will overestimate the stress at the crack tip and will lead to calculation errors when comparing to LINKpfat. The post-processor will be able to give a more accurate representation of the stress as the crack grows because of representative data at each node in the crack growth direction. The pit opening will also grow faster than the pit front due to higher stress and re-evaluation of the geometry factor at both *a* and *c*, see Figure 19. Resulting in a decreasing a/c-ratio.

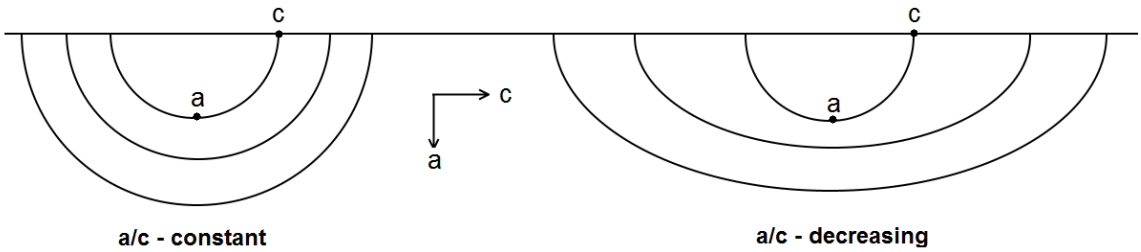

Figure 19: Simplified crack growth possibilities with initial a/c = 1.

While the effect of bending on the crack growth in LINKpfat is interesting in itself, this was previously covered by another master thesis written by Løtveit and Rasten in spring 2014 [37]. The final crack depth for the fatigue calculations was set to 2 % of the blade thickness instead of 50 % as for Case 1 to mitigate the effect of the decreasing stress field. This allows for comparison between the manual calculations and LINKpfat without extensive reworking of the stress intensity equation used in Excel.

Table 6: Parameters used to calculate corrosion pitting fatigue on simplified turbine blade in bending.

Parameter	**Value**	**Component geometry**
Blade length l [mm]	500	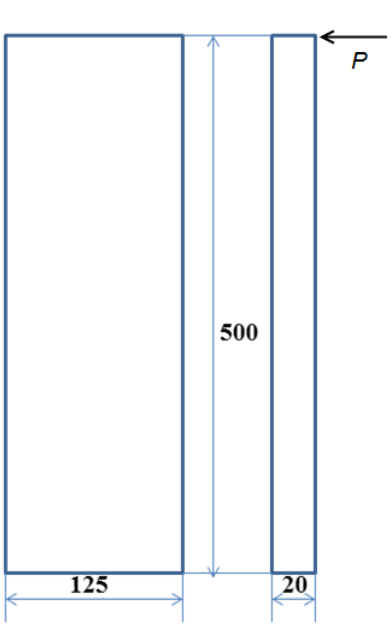
Blade width w [mm]	125	
Blade thickness t [mm]	20	
Final crack depth a_f [mm]	0,4	
Lognormal dist., scale parameter σ [mm]	0,48876	
Lognormal dist., location parameter μ [mm]	-3,6748	
Defect density z_0 [pits/cm^2]	1	
Loading force P [N]	3000	
Max bending moment M_b [kNm]	1500	
Max tension stress [MPa]	180	
Paris mat. constant C [(m/cycle)/(MPa m^{0,5})^m]	1,1*10^{-11}	
Paris mat. constant m	3,37	
Geometrical factor F	1,12*(2/π)	

Abaqus 6.13 model

The same Abaqus model as in Case 1 was used, but the mesh was made finer in the lengthwise direction to ensure a more detailed stress distribution across the investigated front surface. Loading conditions were defined to be as similar to the loading case in Figure 18. Loads were modelled so that there would not be highly stressed nodes at the edges that could interfere with the fatigue calculations. All nodes on surfaces not on the front side were defined to be free of corrosion pitting in the input file. The model and the stress results for the front surface are shown in Figure 39, Appendix B.2. All input parameters used shown in Table 6.

Pit depth distribution

An important assignment for the thesis was to look for corrosion pit depths and surface density found on real-life applications. This was a challenging task, because finding complete datasets for corrosion pit depths proved to be difficult. The best source for raw data for this Case was corrosion pits on gas-turbine blades from a journal article describing a new method to characterize pit depths [13]. It included histograms for the two zones on turbine blades shown in Figure 20 at running hours of 24 000 and 41 000 hours.

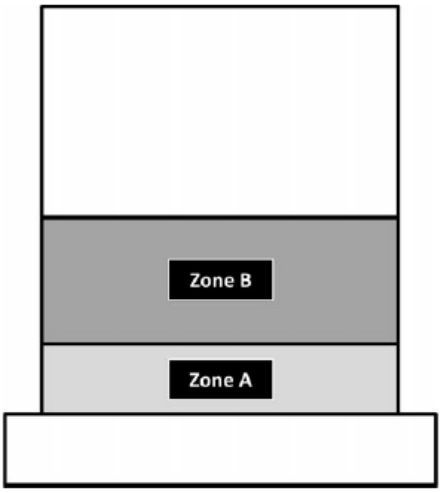

Figure 20: Zones used to distinguish criticality of pits [13].

LINKpfat can consider the component as two parts in v.1.2.0.9, one with surface defects and one without. It was thus not possible to use two defect distributions for different zones of the blade. This case addresses the critical defect chosen in a linearly decreasing stress field and is not a comparison to fatigue data of a real case. Zone A data for one of the turbine blades was used to represent the entire surface. This is of course not a statistically representative way to use this defect distribution, but allows the use of a real pit depth distribution a turbine blade could experience. EasyFit 5.6 was used to fit the data extracted from the pit depth histograms presented in the article. The chosen histogram has the highest density of defects and was from the 1st stage blade no. 2 with 41 000 running hours. A comparison between the three defect distributions that best represents the data is shown in Figure 21.

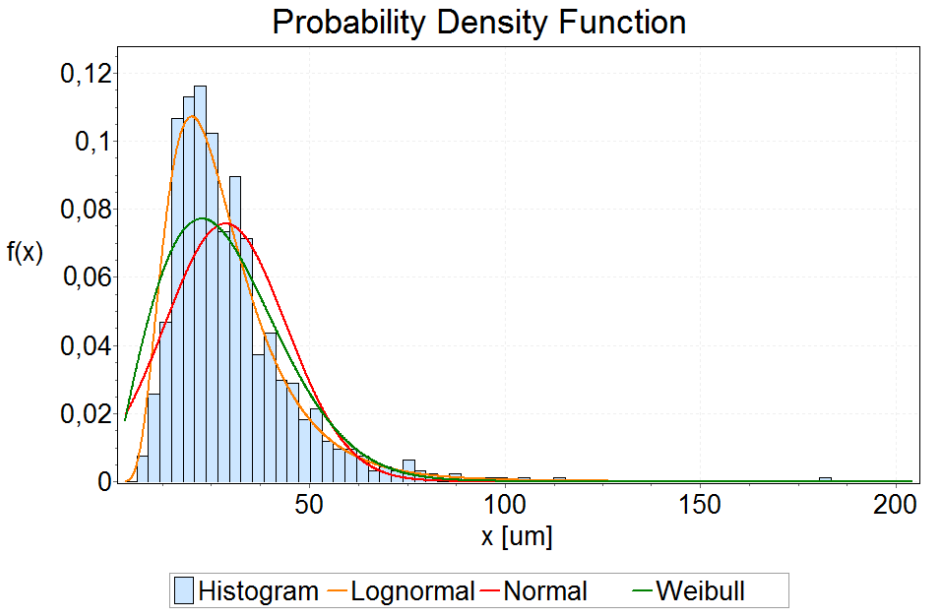

Figure 21: Comparison between the best fitting distributions [33]. Note: f(x) refers to the histogram, not the distributions.

Lognormal gave the most accurate representation of the pit depth population. The PDF and CDF equations for the lognormal distribution are given in Appendix A.1. A graph for the CDF for the lognormal distribution used to generate the depth of the defects is shown in Figure 40 in Appendix B.2.

Defect density

Defect density is given for this sample to be 15,2 pits per square millimetre [13] in Zone A of Figure 20. There is no reference to how large this sample area is. Zone B above has a generally lower defect density. For the other blades in this article, lower densities are reported. Pit density is also affected by whether or not it is a stage 1 or stage 2 blade. An average number of pits of 15,2 per square millimetre found on a limited zone on one blade will not be statistically representative for a larger number of samples, nor would it be correct to apply this density to the entire surface. A decision was made to use a lower defect density for the entire surface that kept the number of defects on a manageable level for the calculation's sake. The defect density was stated as important for the thesis, but has for this particular Case been switched for a more computationally reasonable number. A defect density of 1 pit per square centimetre will be used in this case which results in a mean number of defects drawn to be 625. A correct defect density for the investigated component will be used when testing the post-processor against fatigue life testing in Case 3 in Chapter 6.

5.3.2 Calculation results

This section provides the results for ten components for each calculation method. In this case, the location and selection of the critical defects are the main objectives to be investigated. Results for each calculation method are presented in separate tables and location figures for an easier comparison.

5.3.2.1 Manual calculation

The critical defect for each component and their location is presented in Table 7. The depth of the critical defect is given in addition to its rank among all the defects generated. A rank 7 defect is the seventh largest defect drawn. Full calculation for component #1 is shown in Table 25, Appendix B.2 showing the results for all 24 section of the blade.

Table 7: Results for the ten components calculated manually.

#	Defects	a_i [µm]	Crit. def. rank	N_f [cycles]	Location
1	633	119	1	$7{,}24 * 10^5$	21
2	588	73	7	$7{,}87 * 10^5$	24
3	659	69	6	$8{,}34 * 10^5$	24
4	617	105	1	$6{,}15 * 10^5$	23
5	645	84	6	$7{,}87 * 10^5$	23
6	628	102	3	$1{,}03 * 10^6$	20
7	620	68	15	$8{,}46 * 10^5$	24
8	613	109	2	$5{,}08 * 10^5$	24
9	584	59	29	$9{,}73 * 10^5$	24
10	670	112	1	$6{,}64 * 10^5$	22
Average	625,7	90	7,1	$7{,}77 * 10^5$	-
Range	86	60	-	$5{,}21 * 10^5$	-
PRR	13,7 %	50 %	-	67 %	-

As expected the range of critical defects are much larger than for the pure tension case. Results show a greater dependency on the stress than on the critical pit depth. This results in most critical defects being located in the high stress zone at the restrained end of the blade. A more thorough discussion is given in Section 5.3.3. Figure 22 gives a visual representation of the location of the critical defects for each component. The results for the manual calculations show which regions to expect most of the critical defects and a tentative critical defect limit line. Above this line there is a very low probability of the corrosion pits being critical.

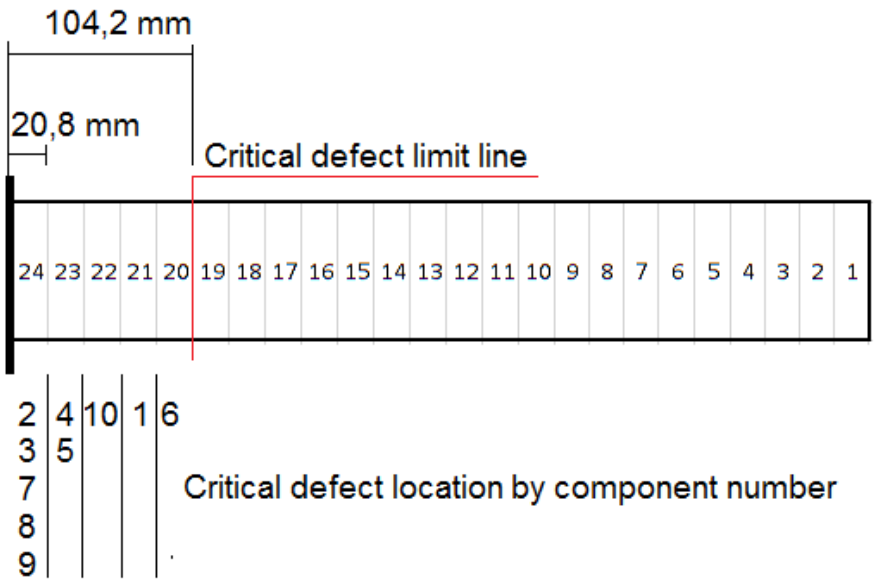

Figure 22: Critical defects and their location on the top surface of the turbine blade.

5.3.2.2 LINKpfat v.1.2.0.9 results

The critical defect for each component and their location is presented in Table 8. Critical pit location is marked in Figure 23. A location column is added with the values inside/outside in reference to the estimated critical defect limit line found in the manual calculations.

Table 8: Results for the ten components with LINKpfat v.1.2.0.9.

#	Defects	a_i [µm]	N_f [cycles]	Location
1	581	115,4	$1,68 * 10^7$	Outside
2	641	111,6	$7,56 * 10^6$	Outside
3	628	89,1	$1,71 * 10^8$	Outside
4	658	85,4	$1,33 * 10^6$	Inside
5	600	122,9	$7,69 * 10^5$	Inside
6	635	103,2	$1,11 * 10^6$	Outside
7	622	115,5	$4,95 * 10^6$	Outside
8	612	135,8	$1,59 * 10^8$	Outside
9	650	96,4	$4,51 * 10^6$	Outside
10	659	95,4	$1,37 * 10^6$	Inside
Average	628,6	107,1	$3,78 * 10^7$	-
Range	78	135,8	$1,71 * 10^8$	-
PRR	12,4 %	47,1 %	450 %	-

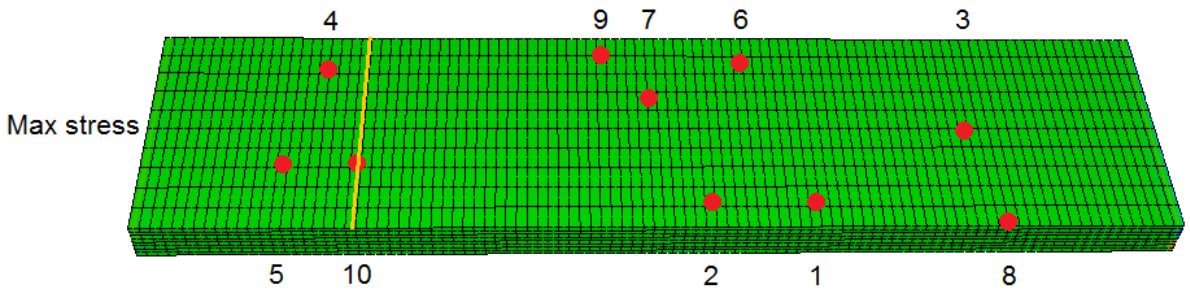

Figure 23: Critical defect location for each component. Closest number for each red dot corresponds to the component number. Yellow line represents the theoretical defect line limit from Figure 22.

Critical defect size and number of defects were drawn are within the expected range estimated with the manual calculations. The fatigue life results are on a wider spectrum compared to the manual calculations. Figure 23 explains why this has occurred. Life determining defects are seemingly arbitrarily distributed across the entire surface with only three of them falling within the expected critical area. An investigation into the cause of these incidents is presented in the next section.

5.3.3 Results discussion

Results from the two calculation tests does not show the same location overlap in results as expected. Defect generation, amount and critical defect distribution, seem to be consistent with Case 1 and will be considered to be working as intended. An investigation in needed to find out why the critical defects in the LINKpfat case is located across the entire surface instead of within a zone near the clamped side with maximum stress. When comparing the fatigue lives for the defects LINKpfat considered critical and the fatigue lives of defects in the corresponding section for the manual calculations, the cycles needed to reach the critical state seem to be reasonable. Table 25 in Appendix B.2 can be used for comparing the expected fatigue life at the location of the LINKpfat defects. The stress situation was found to be more influencing than the fatigue distribution, with the current defect density, in the manual calculations. Comparing the location of critical defect in component #3 in the LINKpfat case to the location of all generated defects for this component, see Figure 41 in Appendix B.2, it is very probable that there are several larger defects at a location with a higher initial stress. A shorter fatigue life for component #3 is quite likely if LINKpfat had calculated the full fatigue life for nearly any of the defects located at higher initial stress. The most likely cause for the apparent randomness when choosing the life determining defect must thus be the method the software determines the

critical defect. As mentioned in Chapter 3 the way the software does this is calculating the initial crack growth rate *da/dn* for all the generated defects. Something in the way the program determines this seem to be malfunctioning when there is a variable stress situation. A request was made to LINKpfat developer Vidar Osen to examine this portion of the code. Version 1.2.0.10 was updated to fix this issue. The next section provides a re-calculation of the case with the newer software.

5.4 Case 2b - simplified turbine blade subjected to bending (pfat v1.2.0.10)

This chapter is a recalculation of the LINKpfat part of Case 2a. All input are the same, the only difference is the changes made to the initial defect evaluation in version 1.2.0.10.

5.4.1 LINKpfat calculations

The critical defect for each component and their location is presented in Table 9. Critical pit location is marked in Figure 24. A location column with the values inside/outside in reference to the estimated critical defect limit line found in the manual calculations is kept for this version to show that the issue seems to be fixed.

Table 9: Results for the ten components with LINKpfat v.1.2.0.10.

#	Defects	a_i [µm]	N_f [cycles]	Location
1	553	71,3	$1,45 * 10^6$	Inside
2	615	68,2	$9,03 * 10^5$	Inside
3	614	74,6	$8,55 * 10^5$	Inside
4	628	72,6	$1,02 * 10^6$	Inside
5	625	60,1	$1,03 * 10^6$	Inside
6	620	73,8	$9,70 * 10^5$	Inside
7	636	98,7	$1,28 * 10^6$	Inside
8	624	94,1	$6,16 * 10^5$	Inside
9	599	84,6	$9,82 * 10^5$	Inside
10	660	92,1	$9,22 * 10^5$	Inside
Average	617,4	79,0	$1,00 * 10^6$	-
Range	107	38,6	$8,35 * 10^5$	-
PRR	17,33 %	48,9 %	83,3 %	-

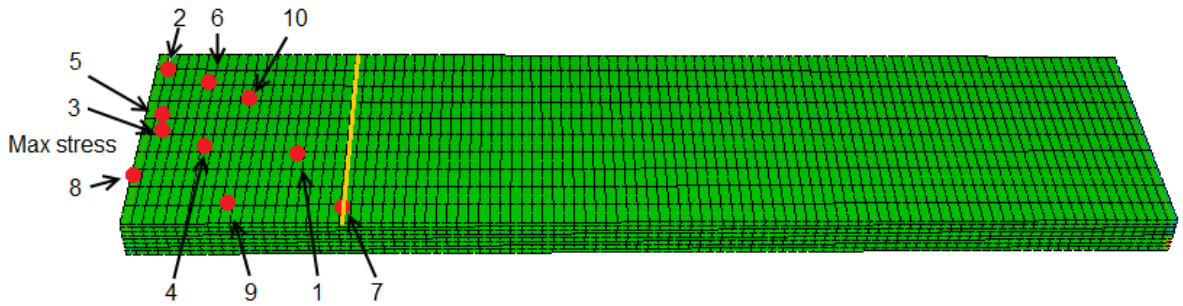

Figure 24: Critical defect location for each component. Yellow line represents the theoretical defect line limit from Figure 22.

All defects are in this version found within the expected region estimated in with the manual calculations.

5.4.2 Results discussion

Comparing the critical defect locations found in version 1.2.0.9 against the critical defect locations found in 1.2.0.10 shows an improvement compared to the estimate made with the manual calculations. The problem with the initial crack growth evaluation seems to be resolved in the new version.

Table 10: Results from Table 7 and Table 9 compiled for ease of reference.

	Manual calculations			**LINKpfat (v.1.2.0.3)**		
#	**Defects**	**a_i [µm]**	**N_f [cycles]**	**Defects**	**a_i [µm]**	**N_f [cycles]**
1	633	119	$7{,}24 * 10^5$	553	71,3	$1{,}45 * 10^6$
2	588	73	$7{,}87 * 10^5$	615	68,2	$9{,}03 * 10^5$
3	659	69	$8{,}34 * 10^5$	614	74,6	$8{,}55 * 10^5$
4	617	105	$6{,}15 * 10^5$	628	72,6	$1{,}02 * 10^6$
5	645	84	$7{,}87 * 10^5$	625	60,1	$1{,}03 * 10^6$
6	628	102	$1{,}03 * 10^6$	620	73,8	$9{,}70 * 10^5$
7	620	68	$8{,}46 * 10^5$	636	98,7	$1{,}28 * 10^6$
8	613	109	$5{,}08 * 10^5$	624	94,1	$6{,}16 * 10^5$
9	584	59	$9{,}73 * 10^5$	599	84,6	$9{,}82 * 10^5$
10	670	112	$6{,}64 * 10^5$	660	92,1	$9{,}22 * 10^5$
Average	625,7	90	$7{,}77 * 10^5$	617,4	79,0	$1{,}00 * 10^6$
Range	86	60	$5{,}21 * 10^5$	107	38,6	$8{,}35 * 10^5$
PRR	13,7 %	50 %	67 %	17,33 %	48,9 %	83,3 %

When comparing the fatigue results for the manual calculation and version 1.2.0.10 in Table 10, the results seem consistent and within the expected level of variance due to the sample size and distribution parameters. Comparing the average fatigue life between the two shows that the RDA calculations indicate a 28 % higher fatigue life. LINKpfat uses the exact stress level at the pit location, while the manual solution uses the average for the section were the pit is located on. The decreasing stress through the section also plays a part, this was mitigated by keeping final crack depth to a minimum. Component thickness is also a factor that is considered in LINKpfat along with a recalculation of the geometry factor as the crack changes its width to depth ratio. A combination of these factors are the most likely reason the calculated fatigue life has a higher difference than in Case 1. Poisson and lognormal distributions give relatively similar results in both cases and a larger sample size would probably make the results on that section even closer. There is no expected issue in the results for the defect generation part. The percent relative range in the three parameters being compared is quite close and would be closer with a larger sample size. A comparison between the size rank for the critical defects could be interesting to investigate, but LINKpfat does not have an accessible method to check the size of all generated defect.

5.5 RDA verification conclusion

Case 1 and 2a/b has provided a verification of several aspects of the Random-Defect. By comparing the results for simple components given by LINKpfat and manual life predictions, several new iterations of the software have been developed. Issues regarding performance, calculation of the initial critical defect was corrected and the newly added option to define a specific area of the component attacked by surface defects have been tested. The defect generation part of the software; size, number and location seem to give results consistent with the manual calculation tool. Fatigue life calculations show some degree of discrepancy between the two calculation methods. Several reasons have also been stated in the discussions in the previous sections. The manual model is a somewhat simpler implementation of the fatigue crack calculation than LINKpfat's which takes into account the changing crack geometry and component thickness. Stress values used in calculations are also sensitive to how well the component has been defined and modelled in the FEM-analysis tool. Some more tests should also be conducted to verify that the initial critical defect LINKpfat chooses when performing the calculation has been properly addressed with the newer versions. All these reviews are kept in mind when comparing a LINKpfat calculation to a fatigue test on specimens with pitted data.

6. Case 3 – LINKpfat compared to fatigue test data

The previous chapter helped verify LINKpfat for application on simple components with randomly distributed corrosion pits. Continuing this verification, a calculation test will be presented in this chapter where LINKpfat results are compared to fatigue test data from components attacked by corrosion pitting. When looking for corrosion pit fatigue testing it was difficult to find data sets that included all necessary calculation inputs. While there are several published articles on the topic, mainly on aircraft applications, many were lacking some information needed to properly define the testing conditions and the pit metrics. The most complete set that was in a fatigue testing project done by DSTO on an F-111 aircraft wing component [18]. It included tests on various stress levels and included enough data to characterize most inputs adequately. All input parameters are discussed in the next section, followed by fatigue calculations compared to the test data. Sensitivity analysis on certain parameters is also done to check which has the most influence on the LINKpfat results.

6.1 Fatigue test presentation

The report includes fatigue calculations on high and low stress concentration specimens, high-Kt and low-Kt, subjected to constant amplitude and spectrum loading. Case 3 focuses on the high-Kt results for constant amplitude loading because LINKpfat only allows for this loading case. The low-Kt testing did not have corrosion pits. DSTO had a limited number of specimens available and several types of tests, leaving only five specimens for high-Kt constant amplitude loading with corrosion pitting attacks. The specimens were meant to emulate the stress concentration and stress gradient in a fuel flow venthole located in the wing of an F-111 aircraft. Testing was conducted at 10 Hz with a 250 kN Instron load frame in laboratory air [18]. Specimen geometry is shown in Figure 25. A more detailed view of the oblong hole geometry is shown in Figure 42, Appendix C.1.

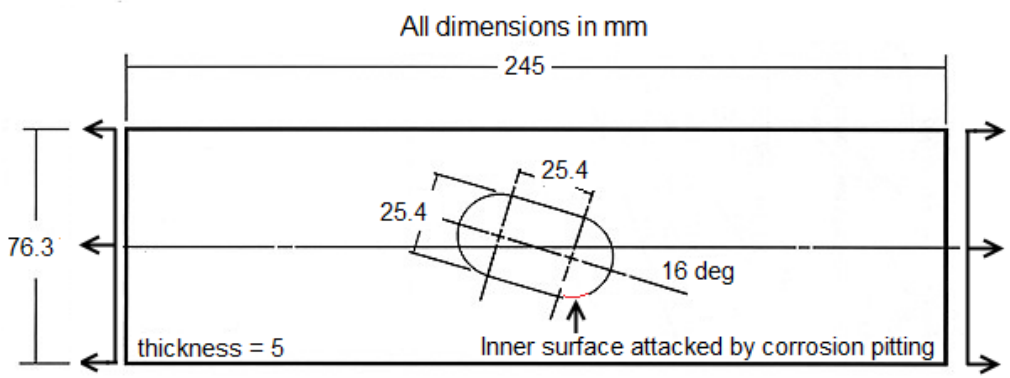

Figure 25: The specimen geometry used in the fatigue testing. Note: some of the components were surface ground with and had a thickness of 3,81 mm [18]. Corrosion area discussed in Section 6.2.3.2.

D6ac high strength alloy steel is the material used for this component and the material data used is presented in Table 11. Testing was done at four different stress levels. The peak stress was assumed to be at a location in the oblong hole with a stress concentration factor of 4. Two of the peak stresses levels, 896 and 1144 MPa was within the elastic loading limit. At 1310 and 1386 MPa the stress situation goes from close to monotonic yield to well developed plasticity in the latter case. The load ratio during testing was R = 0,1. Inaccuracy may occur at these levels depending on the level of plasticity, which could be analysed with Neuber's rule. For this calculation routine elasticity is assumed even though it will be incorrect to some degree.

Table 11: Material data for D6ac steel [16].

σ_{UTS} [MPa]	σ_{ys} [MPa]	ΔK_{th} [MPa√m]	K_c [MPa√m]	K_{Ic}(low) [MPa√m]	K_{Ic}(high) [MPa√m]	E [MPa]	v
1517-1655	1310	2,2	122	46,5	74,1	210 000	0,32

Fatigue results for the five specimens tested at constant amplitude loading is presented in Table 12. Remote stress is the stress level in the section of the component furthest from the stress concentration at the hole, experiencing close to uniform stress.

Table 12: Fatigue test results for the specimens tested at R = 0,1.

Specimen number	Remote stress [MPa]	Peak stress [MPa]	Max pit depth [µm]	Fatigue life [cycles]
FP82AC	224	896	93	48137
FP81AD	224	886	74	64253
FP85AD	286	1144	92	19784
FP85AF	327,5	1310	87	11510
FP85AE	346,5	1386	81	8950

6.2 Calculation input

This section provides the calculation input used to best address the test conditions and material behaviour of the fatigue testing. Limitations for each part are discussed in the respective section. Discussion includes Abaqus input such as loading, geometry, boundary conditions, material definition and meshing in Section 6.2.1. Pit distribution parameters that best captures the pitting situation described in the report is discussed in Section 6.2.3.1 and 6.2.3.2. D6ac crack growth models are evaluated and described in Section 6.2.2.

6.2.1 Abaqus 6.13 model

The Abaqus model was designed after the general drawing in Figure 25 in the previous section and the detail sketch of the oblong hole shown in Figure 42, Appendix C.1. A thickness of 5 mm is shown on the sketch, but the report indicates that most of the specimens were surface ground to a thickness of 3,81 mm. The latter thickness was used for the Abaqus model used on all stress levels. It is not explicitly stated for each component number in the report what thickness were used, but it is assumed that the five specimens used for high-Kt constant amplitude testing was of this thickness.

An Instron 250 kN load frame was used. Peak stress for each load level was used to calculate the loading force applied to the specimens. The peak stress in the report was assumed to be caused by a stress concentration factor *Kt* of 4. Applied load for Abaqus loading was thus the force needed to generate this level of remote stress on the cross section furthest away from the hole. Several methods for applying the correct load was tested to check the impact of having some degree of freedom on the end the load was applied to. In each method, one end of the specimen was held firm. The three methods tested were; defining a surface load as uniformly affecting the surface, both ends locked by boundary conditions while one end was given a

displacement value in the loading direction, and a master/slave system between all nodes on the top surface with some degrees of freedom locked. The second method is the one most similar to how the loading would be applied in the testing instrument. Each method gave the exact remote stress, and the peak stress area around the hole gave little variance, at most 1-2%. The uniform stress method was used as it was most computationally effective and was very similar to the other methods. Horizontal and vertical displacement was very low in all cases.

Different mesh densities were tested, and a mesh width of 0,5 mm was used for the edges of the oblong hole and its surrounding areas to ensure accurate stress distributions in the pitted area. Quadratic elements C3D8 and C3D20 with and without reduced integration were tested. C3D20 without reduced integration gave the best stress convergence results with the given mesh and enabled more nodes in each element for LINKpfat to utilize when considering crack growth through the element. Figure 26 show the high density meshed areas near the critical parts around the oblong hole. A transitioning area is also seen with some inconsistent meshing. This is in a region that is not as important as input to LINKpfat and does not interact with the stress situation in the critical areas. Mesh verification done by Abaqus accepted all elements as OK.

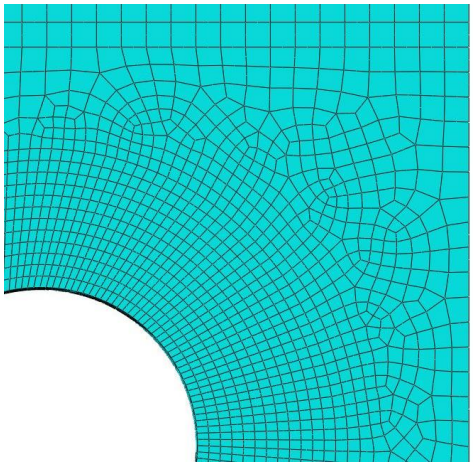

Figure 26: Mesh detail of oblong hole.

Initial modelling of the component was a 1:1 copy of Figure 25. Preliminary testing in LINKpfat led to a discovery of a fundamental error in how LINKpfat considers cracks growing from the edges of holes. When a defect was generated on the edge of the hole the software runs into an issue when calculating the distance to the nearest surface. As explained by Vidar Osen the software will in this case find the distance to the surface on the other side of the hole. In some specimens this lead to the creation of defects that were not entirely defined as attached to the

surface and thus assumed to be embedded defects. This lead to performance issues with calculations taking several hours instead of minutes. Results were also very unreliable. This was a known problem for the LINKpfat team and the proposed workaround was to model only one half the component. This leads to some modelling inaccuracies because the oblong hole is slanted and is antisymmetric both horizontally and vertically. It was decided to model half the component cut in the middle of lengthwise direction and define the left edge with symmetry boundary conditions. A comparison of the stress results between a full model and the proposed "symmetric" model is shown in Figure 27.

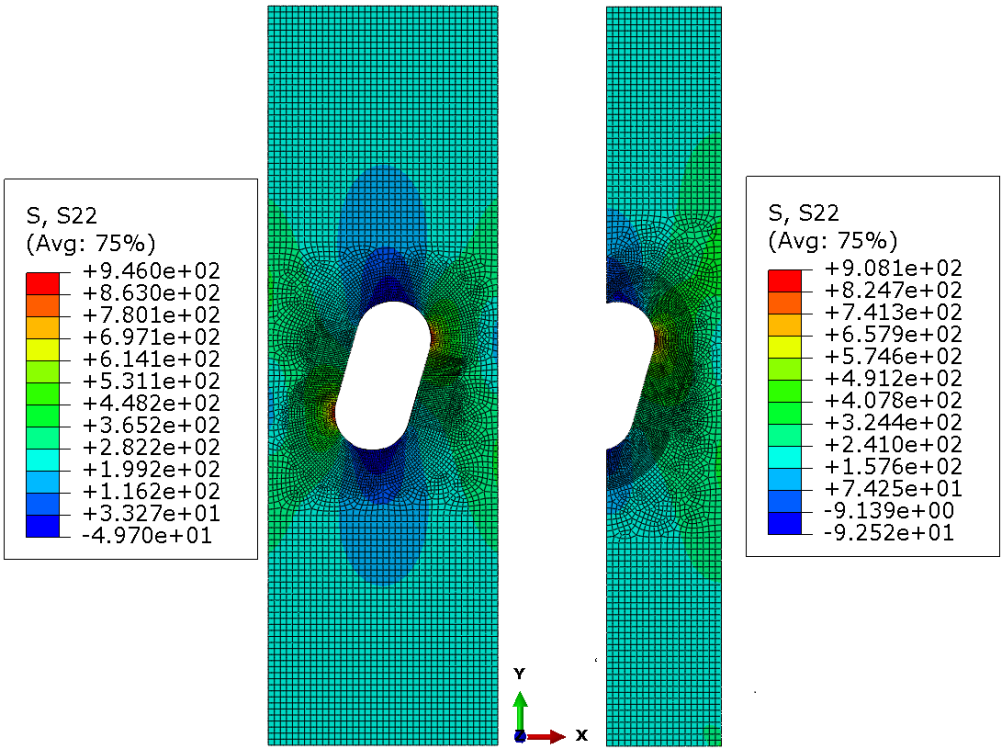

Figure 27: Comparison between the full model and the same model with a symmetry plane along the y-axis for the remote stress of 224 MPa. Units shown in the stress legend is MPa.

The full model stress analysis indicate a *Kt* of 4,22, resulting in a peak stress difference of 5,5 % compared to the estimated peak stress from the DSTO report. When using the imperfect solution of a symmetry plane to help LINKpfat generate surface-defects correctly, the peak stress is only 1 % higher than the one reported. It is not stated why the peak stress is assumed to be four times higher than the remote stress. The full-scale Abaqus model could be correct or have some error that causes it not to properly represent the real fatigue test. The symmetry-model has the most "correct" results compared to the DSTO report, but due to the antisymmetric nature the stress distribution in the rest of the component does not match the pattern found in the full scale model. How the stress gradients in each case compares to the test specimens is also of concern that was

could not be validated. For LINKpfat purposes only a limited area is of interest and the results for this region seem to be in good agreement with the desired peak stress values in the DSTO report. In Table 13 the four investigated stress levels are shown along with a cropped image of the stress situation found in the Abaqus models for each in Figure 28.

Table 13: Stress comparison for reported stress in DSTO report and the symmetric Abaqus 6.13 model.

	DSTO report		**Abaqus 6.13 model**	
Level	**Remote**	**Peak**	**Remote**	**Peak**
1	224	896	224	908
2	286	1144	286	1159
3	327.5	1310	327.5	1328
4	346.5	1386	346.5	1405

The symmetric solution has a peak stress difference of 1%. Because of the difference in peak stress levels between the full model and the symmetry-model, some caution is needed when interpreting the LINKpfat results because the Abaqus input is not necessarily a perfect representation of the stress situation in the fatigue test specimens.

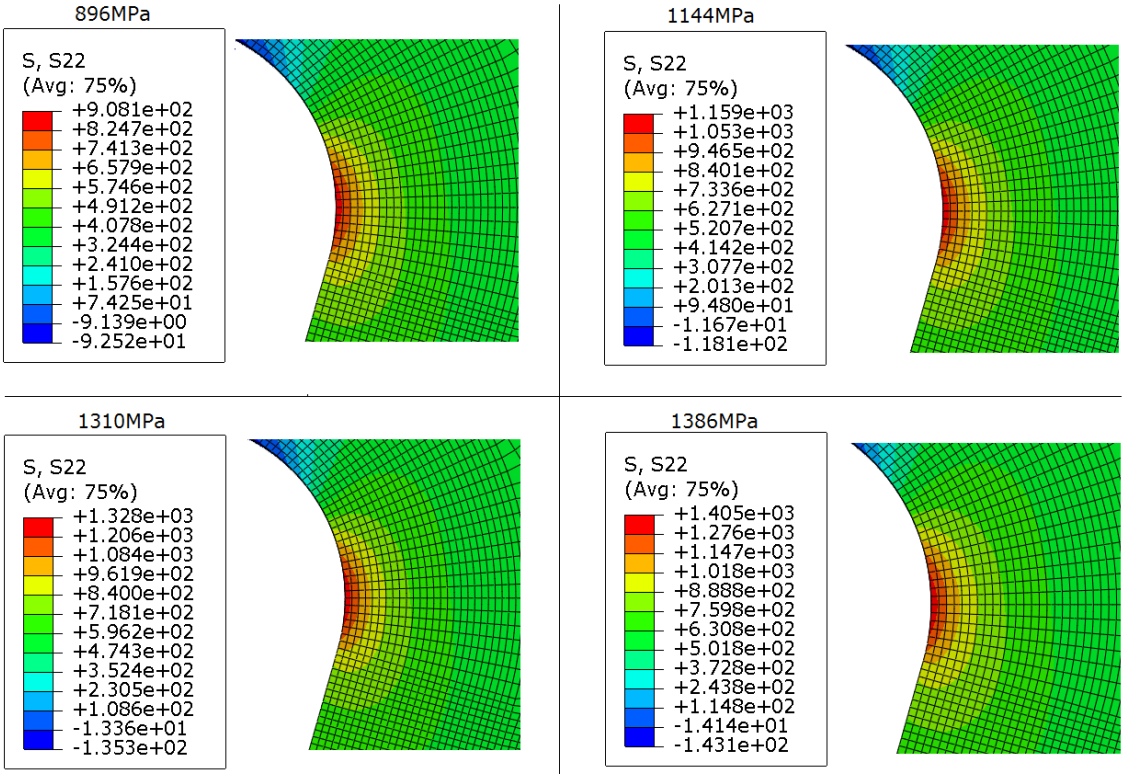

Figure 28: Stress situation in location of peak stress that is also attacked by corrosion pitting.

6.2.2 Crack growth curves

Crack growth in D6ac steel needs to be described by an appropriate curve that fits the expected rate the cracks will grow. In the DSTO report [18] two curve fits are proposed based on data from Feddersen et al. gathered in a paper on the crack behaviour in D6ac steel for F-111 aircraft in 1972. The original document was unfortunately not found online to be used as a reference. One of the models was a fit based on the Forman equation shown in Equation (12).

$$\frac{da}{dN} = \frac{C(\Delta K)^n}{(1-R)K_c - \Delta K} \tag{12}$$

The Forman curve for D6ac steel has two different sections based on the given stress intensity. From threshold to 14,2 MPa√m (13 ksi√in) Equation (13) applies, and for stress intensity higher than this, Equation (14) applies. Note the units are in ksi and inches. LINKpfat does not support other crack growth formulations than Paris Law. To circumvent this limitation, the Forman equation was used to calculate the crack growth rate from the stress intensity threshold to 100 ksi√in and converted to SI units afterwards. A total of 194 data points was generated and used as input for the crack growth formulation in LINKpfat. The software will calculate the Paris constants *C* and *m* between each data point, resulting in a Paris curve comparable to the two sections of the Forman fit. To check if this was a decent solution, linear regression was done in Excel for several increments of the curve, which gave R-squared values of 1, indicating a very good fit.

$$\frac{da}{dN} = \frac{7{,}710 * 10^{-9}(\Delta K)^{3{,}655}}{(1-R)110 - \Delta K} \;\; if \;\; (\Delta K_{th} < \Delta K \leq 13ksi\sqrt{\text{in}}) \tag{13}$$

$$\frac{da}{dN} = \frac{1{,}456 * 10^{-7}(\Delta K)^{2{,}497}}{(1-R)110 - \Delta K} if \;\; (\Delta K > 13ksi\sqrt{\text{in}}) \tag{14}$$

This fit is limited to D6ac steel with ultimate tensile strength 1517-1655 MPa, long-transverse (L-T) grain orientation and dry/lab air. The same conditions apply for the second fit, called Modified LMTAS Mean, which is another fit based on the same data set in the document mentioned above. It uses the Forman equation, but has been modified by extending the lower linear portion of the crack growth curve and thus lowering the stress intensity threshold. The

input data was not given, but the tabular data from Appendix A in the DSTO report was used to generate the curve. It has fewer points than the Forman fit, and is for this reason a bit more crude and does not have R-squared values that are as god as the other fit. Both curves are shown in Figure 29 and is how the curves appear when implemented into LINKpfat.

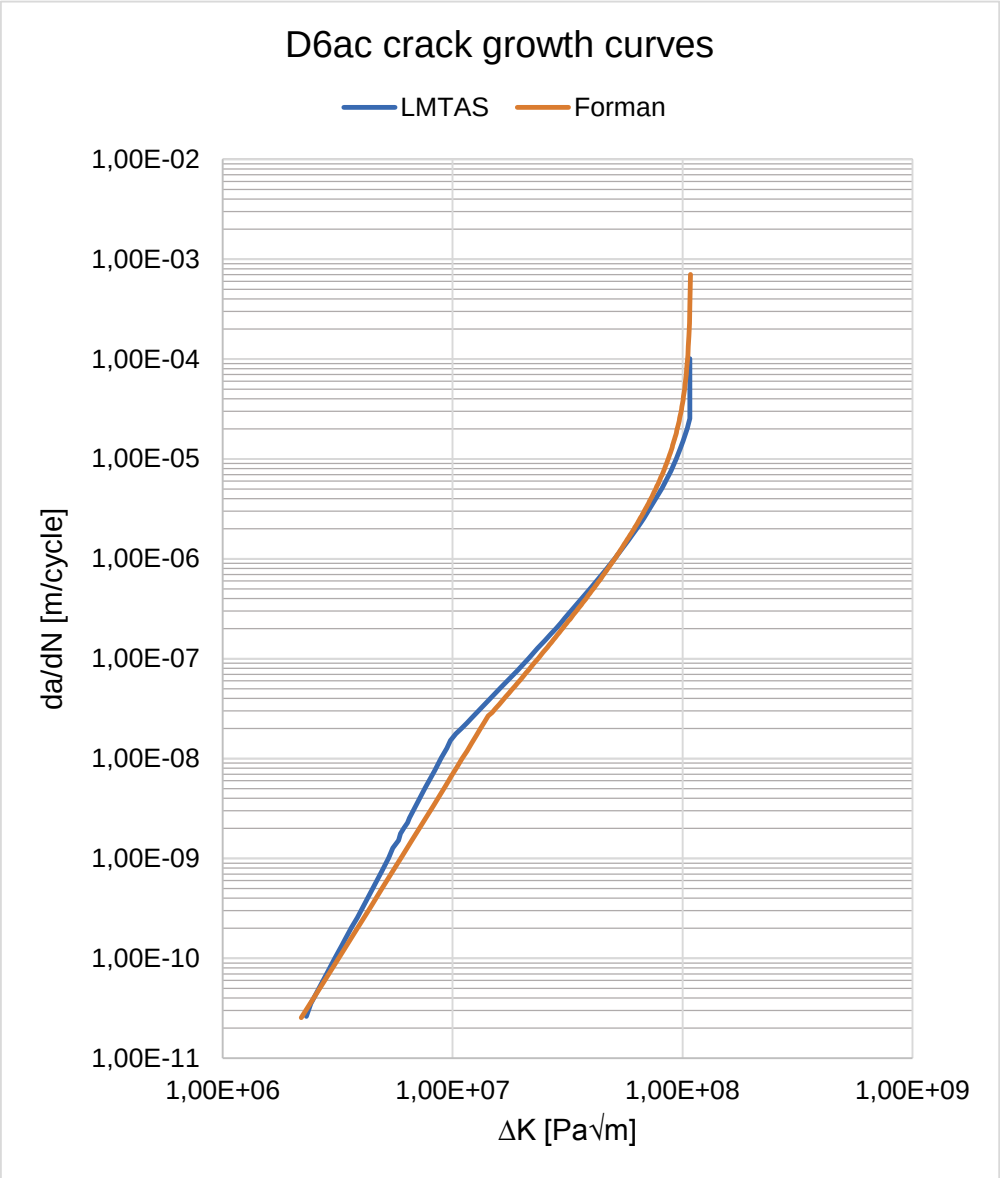

Figure 29: The Forman fit and LMTAS mean fit to crack growth data for D6ac steel.

Both curve-fits were used for calculating the fatigue life and the results are compared in Section 6.3. The Forman fit has a higher number of data points with 194, while the LMTAS Mean had 94 pre-calculated by DSTO. The Forman fit is thus better represented by the approximation made by the Paris curve fit in LINKpfat. An example of the implementation of the Foreman fit in LINKpfat is shown in Figure 43, Appendix C.1.

6.2.3 Pit distribution parameters

This section provides the approximation of pit size distribution for the specimens, how many there is and their attack location. There was not a full dataset available for each specimen that could be used to generate representative pit distribution parameters for each stress level. Data from one or several specimens had to be assumed to be representative for specimens that could have slightly different distribution parameters. These limitations will be further discussed in each sub-section.

6.2.3.1 Corrosion pit size

Corrosion pits were applied to the specimens by laboratory procedures. A hemispherical shape was reported for a large portion of the pits. Having an initial *a/c* ratio equal to 1 in LINKpfat can thus be a good approximation. The report does not include measurements for all pits that appear on each specimen. From the report, pit size distributions could either be created from a histogram containing measurements of 134 corrosion pits during the initial experiments or from the 57 largest pits that appeared on one of the specimens. The histogram was chosen as it had a larger sample size and was deemed more representative of the range of corrosion pits that could occur. Each bar in the histogram had a range of 9 µm and did not include pit depths below 30 µm. The average value for each bar was used as input when generating the distributions.

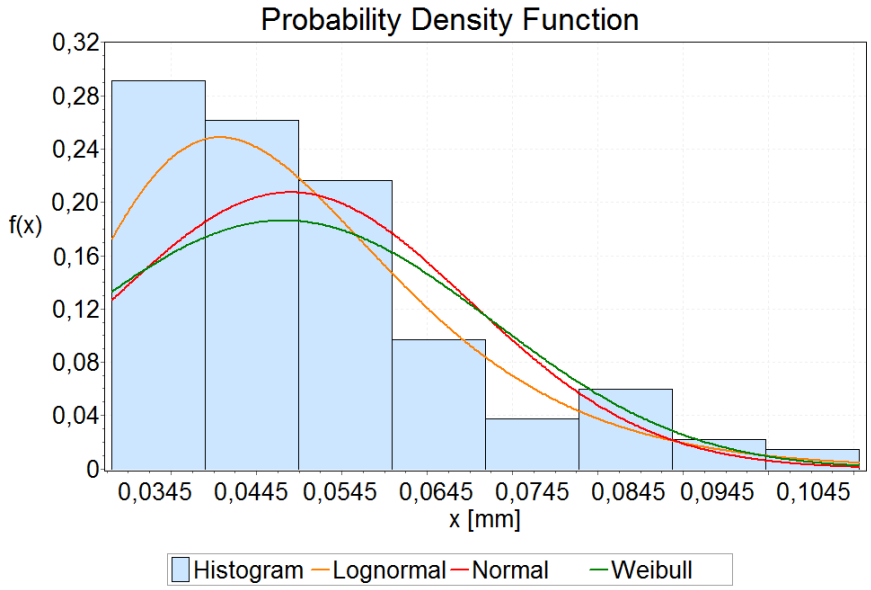

Figure 30: Histogram for pit depths occurring on the specimens and a comparison between the best 3 distribution fits. Note the y-axis f(x) refers to the histogram, not the distributions.

Figure 30 shows a comparison between the three best fits to the 134 corrosion pits measured during the experiments. All three underestimates the probability of the smaller pits in the sample because of the cut-off at 30 µm. The threshold value of 30 µm is a practical application of the extreme value theory proposed by Wormsen et.al. as mentioned in Chapter 4. Lognormal was the best fit for the available data, and will be used for describing the pit sizes on all specimens. More data would likely give a more representative result. To check how much effect the depth distribution has on the final fatigue life some sensitivity analysis will be done in Section 6.4. Table 14 show the distribution parameters for the lognormal distribution in Figure 30.

Table 14: Lognormal distribution parameters for the fit shown in Figure 30.

Scale parameter σ [mm]	Location parameter μ [mm]
0,30086	-3,0194

6.2.3.2 Corrosion pitting attack area

The information available on corrosion pitting area is limited to an analysis that was done on specimen FP78AD. Pits were present in the area of max stress on the inside of the cut-out hole. Pits were mapped 2 mm below the peak stress line, and 6 mm above the peak stress line, see Figure 31. With a specimen thickness of 3,81 mm this gives an attacked area of 30,5 mm^2. Assuming that the 2 and 6 mm distances are along the radius of curvature of the oblong hole, the pitted area in Abaqus was defined as in Figure 31. Geometric equations used to find the corresponding angles for the area definition is shown in Appendix A.2.

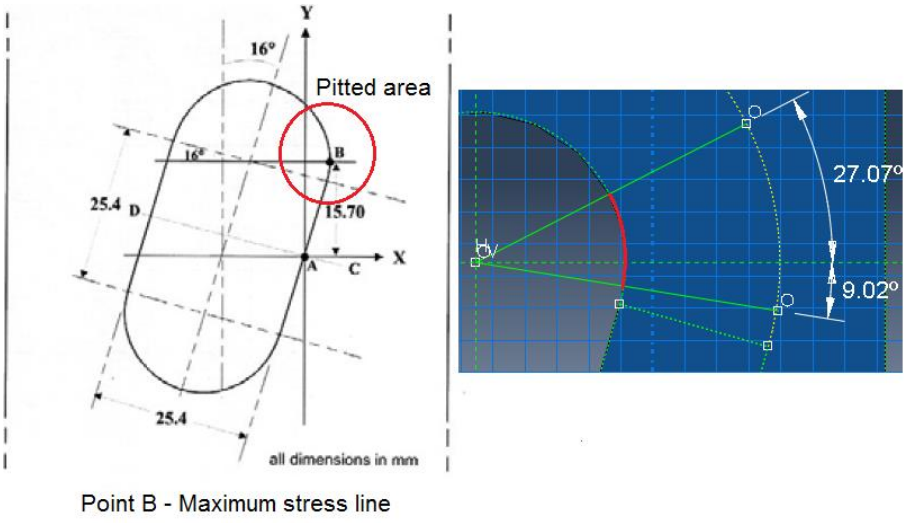

Point B - Maximum stress line

Figure 31: Pitting corrosion attack on the cut-out oblong hole in the peak stress area.

All nodes in Abaqus not on the surface area along the red line in the rightmost figure above were defined as surfaces free of corrosion pits. Basing the pitted area on one example might not be accurate for all specimens. However, the experimental procedure most likely used the same setup and generated pits on the same area. The chosen area by DSTO is thus most likely characteristic for most specimens as long as the defect density within this area is representative. This area is the most highly stressed and based on the calculations in Section 5.4.1 the stress situation has a very large impact on where the critical pits will be located.

6.2.3.3 Corrosion pit density

How many pits occur on each specimen on the area highlighted in the previous section will also be based on DSTO specimen FP78AD. For this specimen, 57 pits over 30 μm were reported. Distributed on a surface area of 30,5 mm^2 the pit density is 1,87 pits/mm^2. Again, defining the pit density on such a limited sample is quite weak, but without any more data it's the only option. Sensitivity analysis is performed in Section 6.4.2 to check how sensitive the fatigue results are to increasing or decreasing number of pits.

6.3 Main calculation results: Forman vs. LMTAS Mean

The fatigue test data only had one or two results recorded for each stress level. To increase the probability that most of the variance that could occur when generating specimens in LINKpfat was captured 100 components were calculated for each stress level. Generating this many components quickly was made possible after a few performance improvements in later versions. Fatigue life range for this simulation would thus have a bigger chance of capturing the possible range a larger test data sample size could give. Abaqus input file and crack growth curves from the previous section are considered constants. A summary of other important input parameters are given in Table 15. The highest K_{Ic} value for the material was used to define the critical crack state. Pit size is described by the lognormal distribution. It was derived from pit sample sizes with a minimum pit size of 30 μm and LINKpfat was given instructions to not draw pits below this threshold. As a test, the maximum pit size was not given an upper value even though the reported max pit depths on the specimens in Table 12 did not exceed 93 μm.

Table 15: Input parameters used for this calculation test. LINKpfat v1.2.0.13.

K_{Ic} (high) [MPa√m]	Min. pit size [µm]	Max. pit size [µm]	Pits density [pit/mm^2]
74,2	30	-	1.87

6.3.1 Results

Table 16 is a summary of the target fatigue lives at the four peak stress levels. Results for the LINKpfat calculation will be denoted by the same peak stress level even though the calculated peak stresses are slightly higher.

Table 16: Summary of fatigue test data and the corresponding peak stress.

Peak stress [MPa]	**896**	**896**	**1144**	**1310**	**1386**
Fatigue life [cycles]	48137	64253	19784	11510	8950

Results obtained from 100 LINKpfat specimens for each stress level is presented in Table 17 for the Forman crack growth curve and Table 19 for the LMTAS Mean curve.

Forman-fit

Fatigue life results for the Forman fit are compared in Table 17 and the corresponding critical pit depths are shown in Table 18.

Table 17: Forman fatigue life results for 100 specimens of each stress level.

Peak stress [MPa]	**896**	**1144**	**1310**	**1386**
Max. fatigue life	30421	15050	8911	8127
Min. fatigue life	14920	7657	4516	3611
Average fatigue life	22052	9636	6078	5173
Standard deviation	2481	1292	654	661
$Nf_{test}/Nf_{pfat\text{-}average}$	2,2 (2,9)	2,1	1,9	1,7

Fatigue life results are mostly consistent across the 100 specimens generated. When comparing the standard deviation to the maximum and minimum fatigue lives it can be seen that there are some statistical outliers. Upon further investigation, it is found that there are very few that lie at the extremes that are shown in the table above. The reasons for this is discussed in the next section.

Table 18: Critical pits that caused the fatigue failures of the Forman-fit in Table 17.

Peak stress [MPa]	**896**	**1144**	**1310**	**1386**
Max crit. pit depth [µm]	209	146	161	199
Min crit. pit depth [µm]	70	66	69	75
Average crit. pit depth [µm]	92	94	95	95
Standard deviation	19	17	14	18

Max critical pit depth does not necessarily correspond to the minimum fatigue life. Location of the critical defect plays an important part in this. The number of pits drawn can be found in Appendix C.2, however it does not give much more information than the numbers drawn are consistent across the various stress levels.

The location of each critical pit for the Forman 1144 MPa is shown in Figure 32. Upper and lower thick black lines indicate the corrosion pitted area. Most critical pits are located in the highly stressed regions with some outliers near the upper boundary.

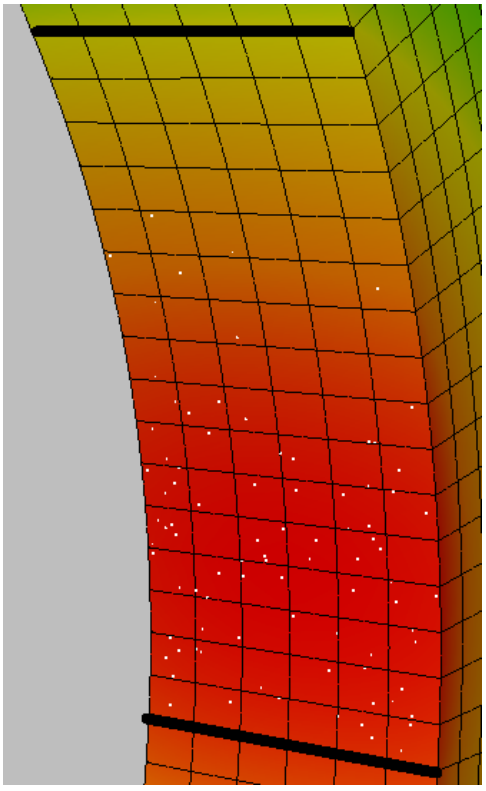

Figure 32: Location of each critical pit for the 100 Forman fit 1144 MPa components. Note: a slight visual bug hides a handful of pits in the most densely populated area depending on the view-angle.

LMTAS Mean-fit

Fatigue life results for the LMTAS Mean fit are compared in Table 19.

Table 19: LMTAS mean crack growth fatigue life results for 100 specimens of each stress level.

Peak stress [MPa]	**896**	**1144**	**1310**	**1386**
Max. fatigue life	30622	14280	7489	7024
Min. fatigue life	12732	4592	4268	2932
Average fatigue life	16770	8186	5293	4320
Standard deviation	2006	1076	578	491
$Nf_{test}/Nf_{pfat\text{-}average}$	2,9 (3,8)	2,4	2,2	2,1

Tables with data on the critical pit depth and number of pits drawn for the LMTAS Mean-fit is found in Appendix C.2. They were omitted from this section because they had results very similar values as the results in Table 18, but were not deemed necessary for the discussion in the next section.

Comparison

Figure 33 gives a visual comparison of the cycles to failure for each crack growth curve and the test data.

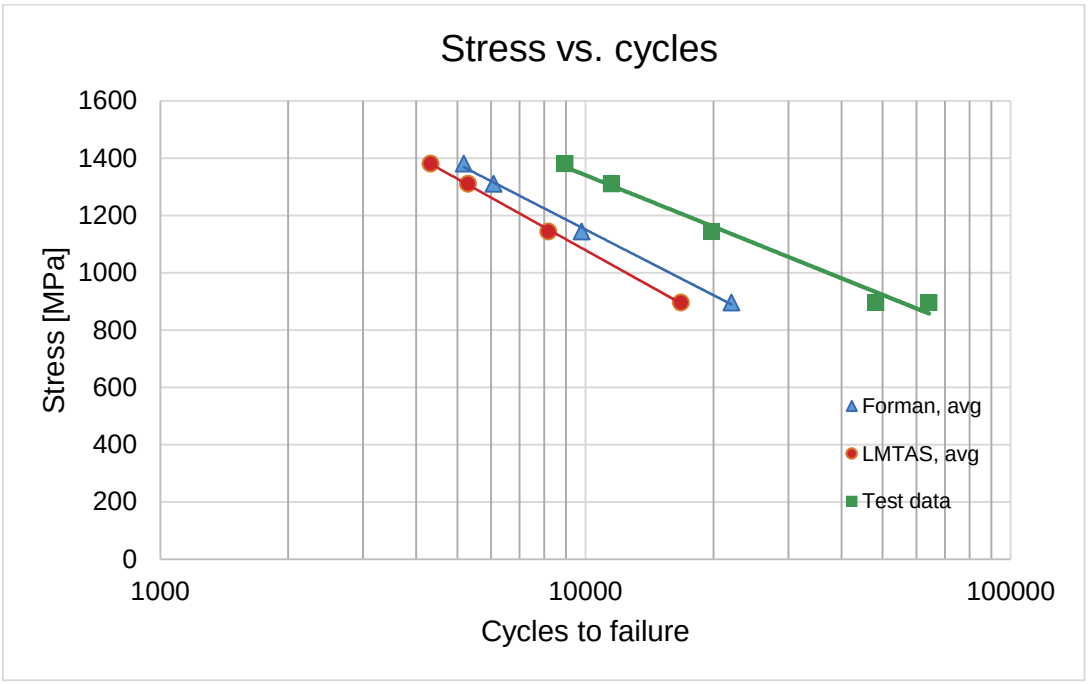

Figure 33: Stress vs. cycles to failure for the average fatigue life results.

6.3.2 Discussion

Fatigue life results indicate that the Forman fit gives the best results compared to the test data. When comparing the crack growth curves in Figure 29, the LMTAS mean fit has a higher crack growth rate in the stress intensity range that most of the crack growth occurs in at these stress levels. As expected the resulting fatigue lives give shorter fewer cycles to failure for this fit. Both does however give quite conservative estimates of the fatigue life. The Forman average fatigue life estimate is off by a factor of 1,7 – 2,2 while the LMTAS Mean misses by a factor of 2,1 – 2,9. Calculation results are influenced by many factors, and a sensitivity analysis on some of the input parameters are done in Section 6.2. Due to the hole-geometry issues with LINKpfat it was not possible to use the full model, which had slightly higher stress levels. This might also have led to results that are more conservative. Forman data gives the best results and will be used in the following sections when checking if which parameters has the most influence on the results.

Many of the fatigue life results are close to the average, but there are a few outliers that give very different maximum and minimum values compared to the expected variance from the standard deviation. One explanation is a combination of very large/small pits being the critical defect, depending on their location compared to the max stress line. To investigate the cause of these outliers, a couple of components for two different stress levels are discussed below.

The location of the critical pit that gives the maximum fatigue life of 15 050 cycles to failure, component #17 in the Forman-fit 1144 MPa peak stress case, was one of them. It is as expected found in a location that is almost as far away from the max stress line that it could get, see Figure 34. Its initial crack size is 102 μm, which is slightly on the larger end of the spectrum, but does not provide the answer to the question of why it was considered the critical pit at that location. Comparing the initial crack size of pits at locations closer to the maximum stress line on several of the other 99 components and their resulting fatigue lives, the component with 15 050 cycles seem very peculiar. It is highly likely that a pit of size comparable to the initial critical pit size of other components and with similar location exists on the specimen with 15 050 cycles. Comparing all critical pit locations in Figure 32 and all generated pits on component #17 in Figure 34 this becomes apparent. A pit of lesser depth at a more highly stressed location should probably be deemed critical, resulting in a lower fatigue life. The software, choosing to calculate the “wrong” critical-pit from the initial crack growth rate for each generated defect could cause this. This was part of the issue in Case2a, and the question remains if this has been 100 % fixed or if the method has a weakness to certain

geometry/loading conditions. It cannot be ruled out 100 % that the chosen pit is the critical one because the initial size and initial crack growth rate for all pits are not readily accessible in LINKpfat. Thus, only the comparison between components can be used as arguments for why it is not necessarily correct. It is however a rare occurrence, with only three other specimens resulting in cycles to failure above 13 000.

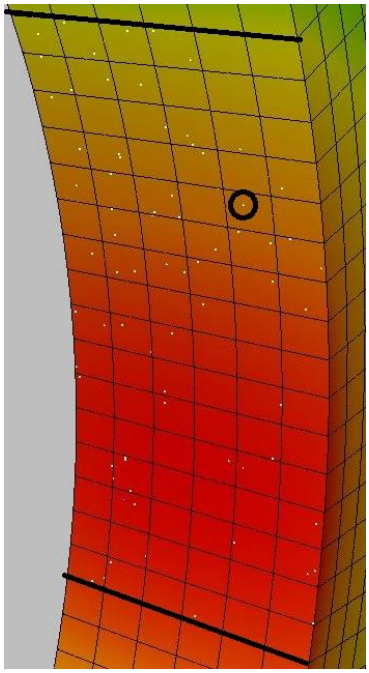

Figure 34: Location of the critical pit on component #17, Forman-fit 1144 MPa. Black lines indicate pitted region.

The minimum fatigue life of 14 920, in the Forman-fit for the 896 MPa stress level is caused by the upper bound having no limit, causing a pit of 200 μm to be located near peak stress. This indicates that not having an upper bound when the control over the experimental are unlikely to produce pits deeper than 100 μm is not correct. Generating a comparably massive pit such as this has a very low probability, and causes some skewing of results. A test was performed in 6.4.1 to check the sensitivity to this input parameter.

Some error might also arise from the hole geometry where the pitting attack is located. The model had to be simplified for LINKpfat to properly address the distance to the closest surface. In the initial testing before the symmetry-plane was introduced to the Abaqus model. A greater scatter was observed in the results, and there was instances of fatigue lives for Forman at 896 MPa peak stress at around 60 000 cycles. Most likely, it is a coincidence that the version with issues generating defects properly had some results that were very close to the test data. This is only mentioned as it could be worth investigating in later validation work.

6.4 Sensitivity analysis

To check how the uncertainty in the inputs could affect the results a simple sensitivity analysis was carried out. In the results of the initial calculations, it was discovered that some very large pits had been generated and considered critical. The largest was unlikely to occur with the carefully controlled environment that were used to create them. A max pit depth limit was chosen as one test. How many pits were generated on each specimen, was also uncertain, and a test was done to check how an increase and decrease in pit density would affect the fatigue results. The critical crack state was also assumed for the material to be on the higher end, therefore a test to check the results for the low and mean K_{Ic} was conducted. Other input parameters were kept the same. To make the investigation manageable, only the Forman crack growth curve was used, and two stress levels were chosen, 896 and 1310 MPa.

6.4.1 Maximum pit depth

To check how truncating of the maximum pit depth that could be drawn from the lognormal distribution would affect the results, three levels were set. 95 μm because it was close to the largest observed pit on the specimens, 120 μm to allow for some larger pits and having no limit like the main calculation.

Table 20: Fatigue life results with pit depth truncated at three different levels.

Stress level [MPa]	**896 MPa**			**1310 MPa**		
Max pit depth [μm]	95	120	∞	95	120	∞
Max. fatigue life	25940	34501	30421	7640	8882	8911
Min. fatigue life	19657	17894	14920	5593	5422	4516
Avg. fatigue life	22106	21995	22052	6287	6266	6078
Standard deviation	1408	2791	2481	387	637	654

From the fatigue life results in Table 20 it can be seen that the average fatigue levels are very similar and show little dependency on the pit depth distribution truncation. There does however seem to be some correlation between the truncation level and the outliers of the fatigue life. Most of the cracks leading to these results initiate from pits above 100 μm. This might indicate as mentioned before that there still is a slight bias for larger defects when picking the critical defect. They do not affect the average fatigue life that was used to compare with the fatigue test data much, but nearly doubles the standard deviation.

Table 21 shows the critical defects for the results above. As expected, all listed values increase gradually, except for the minimum pit size. It indicates that having an unlimited upper boundary does not fit the data all that well because it is unlikely that pits above 150 μm would occur. An upper boundary of 95 μm is used for further testing.

Table 21: Critical pit depth results for the different truncation levels.

Stress level [MPa]	**896 MPa**			**1310 MPa**		
Max pit depth [μm]	95	120	∞	95	120	∞
Max. pit depth [μm]	94	119	209	94	112	161
Min. pit depth [μm]	72	69	70	64	66	69
Avg. pit depth [μm]	84	92	92	84	90	95
Standard deviation	5,8	11,7	18,7	7,1	10,7	14,5

Number of pits drawn for the above data is given in the Appendix C.2, but did not give any unexpected results.

6.4.2 Pit density

The pit density level of 1,87 pits/mm^2 was based on the number of pits on one specimen. This would most likely be different for the other specimens. To check how much this parameter affected the fatigue life results, the standard level was decreased by a factor of 2 and increased by a factor of 1,5. A max pit depth of 95 μm was used for more easily comparable results.

Table 22: Fatigue life results with different levels of pit density.

Stress level [MPa]	**896 MPa**			**1310 MPa**		
Pit density [pits/mm^2]	0,935	1,87	2,805	0,935	1,87	2,805
Max. fatigue life	33263	25940	31381	9569	7640	7581
Min. fatigue life	13896	19657	19752	5735	5593	5534
Avg. fatigue life	22989	22106	22072	6506	6287	6199
Standard deviation	2427	1408	1684	574	387	364

Average fatigue life results indicate a slight increase in cycles to failure when the number of pits are reduced. This is to be expected as the number of pits close to the highest stress levels are fewer and there is a higher probability that critical defects can occur further away. It is consistent on both stress levels, but might also be influenced by the extreme values that occur on a few specimens for each level. The difference is not very large and when compared to the

fatigue test data does not reduce the error compared to the test data any meaningful extent. Assuming a pit density of 1,87 pits/mm^2 for all components is a fair assumption when the resulting fatigue lives are only slightly impacted by very large increases and decreases.

In the maximum pit depth sensitivity test, the cause for the components that had irregular results was thought to be a big pit at location some distance away from the max stress line. In this case, the most likely reason is that these defects are located very near the edges of the component. They are not reclassified as corner cracks and for almost the entire crack growth phase has parts of the geometry outside the component; an example of this is shown in Figure 44, Appendix C.2. Stress intensity calculations may thus not be correct for a larger portion of the calculations compared to the critical defects with results closer to the average. It is however difficult to give conclusive remarks about this without insights into how the software is programmed.

Table 23: Number of pits drawn with the different pit densities.

Stress level [MPa]	**896 MPa**			**1310 MPa**		
Pit density [pits/mm^2]	0,935	1,87	2,805	0,935	1,87	2,805
Max number of pits	47	79	113	40	79	118
Min number of pits	16	42	70	18	41	66
Average number of pits	28,6	57,6	88,4	29,5	58,8	87,9
Standard deviation	5,4	7,7	9,4	4,7	7,6	10

Number of pits drawn are very close to the average values expected at the pit density levels. The Poisson distribution seems well implemented in the software. Even though there are markedly different number of pits, no apparent impact on the size of the critical pits are identified. A collection of the critical pit data can be found in Table 30, Appendix C.2.

6.4.3 Critical crack state

The main calculations used the high K_{Ic} value for the material. A new calculation was completed with the lowest K_{Ic} value for D6ac along with the mean value between the two. Results in Table 24 show the additional cycles to failure with increasing K_{Ic}. For the 896 MPa stress level the average fatigue life increase, 13 percent between the lower and higher values. The 1386 MPa see a nearly 20 % increase. Some of the difference is caused by the different critical crack sizes and locations. Of the three parameters checked with sensitivity analysis, the critical crack state has the most impact. Assuming the highest value to be correct in the main calculations might

make the results slightly better than they should be, if the exact K_{Ic} value for the material been tested.

Table 24: Fatigue life results for the minimum, maximum and mid-level K_{Ic}

Stress level [MPa]	**896 MPa**			**1310 MPa**		
K_{Ic} [MPa√m]	46,5	60,35	74,1	46,5	60,35	74,1
Max. fatigue life	28359	28359	25940	7268	6780	7640
Min. fatigue life	16579	18791	19657	4639	5273	5593
Avg. fatigue life	19512	21359	22106	5253	5881	6287
Standard deviation	2027	1657	1408	437	320	387

6.4.4 Sensitivity analysis overall discussion and conclusion

Changing certain parameters from the main calculation and seeing their effect on the fatigue results has shown that only one of them has any noticeable impact on the results. Parameters concerning the pit size distribution size and number have less impact than the critical crack state. The reason for this is most likely that the area is quite small and the initial defect size is small compared to the final crack size of a few millimetres. Small changes in these parameters will thus have negligible impact on the calculated results. The material parameter of K_{Ic} has a larger impact because it is the determining factor of when the calculations stop. The upper and lower boundary also covers a noticeable range with these stress conditions. Assuming the highest material toughness in the main calculations might overestimate the results slightly, but that is also only by a few percentage points.

7. Discussion

Both corrosion pitting and fatigue are complex subjects on their own, mixing them together makes for a difficult subject to adequately describe all included mechanisms and their interactions. The initial presented theory only discusses the topics briefly and introduce some concepts that show what one need to be aware of when examining the results from the thesis. Corrosion pits and fracture mechanical cracks have different growth mechanisms and interaction patterns that can be very hard to describe easily. There is also a material dependency on both the shape of the corrosion pits and the growth rate for each type of defect. This makes it hard to create a simple all-encompassing model for corrosion pitting fatigue. Crack growth interaction between separate pits/defects can be difficult to take into account and it was therefore proposed a defect density limit on which this model could be applied. These assumptions might reduce the application area for this type of model because corrosion pits occurs on some materials in clusters where it can be challenging to distinguish between separate pit instances. However, in this work, some simplifications had to be made to be able to create a manual model that could be used to validate the LINKpfat post-processor.

Initial application of corrosion pitting fatigue problems to LINKpfat in Case 1 and 2 showed that the software could quite accurately predict the fatigue life response of the components. The probability distribution results on pit size, location and amount gave consistent results when compared to the manual model. Cycles to failure were within 8 – 28 % in the calculation tests. The discrepancy between the tests was most likely due to the simplification of the stress situation in the manual model in Case 2. During the thesis work several new versions of LINKpfat had to be developed, from 1.2.0.3 to the latest version of 1.2.0.14. Several iterations of the software had to be written and published due to odd results and instabilities discovered during the thesis work, and to add the defect free surface feature.

Research to find and identify valuable corrosion pitting fatigue test data that could be applied to the LINKpfat solution was challenging. There is a lot of literature published on the subject, but most of it does not include a full description of all the parameters that were needed to calculate the fatigue life with confidence in all input parameters. The DSTO case had most of the input data required, but some of the assumptions that had to be established were quite weak statistically. Part of this unreliability has been covered and described by the sensitivity analysis. Applying the software to fatigue test data gave relatively good results, with cycles to failure differing by a factor of 1,7 – 2,2 for the best case when compared to the average. Some of the

outliers were deemed critical by the software, resulting in a fatigue life much higher or lower than the average values. Few fatigue test data points were available and the true difference could be higher or lower depending on the variance more tests would generate.

Sensitivity analysis showed that the uncertainty in corrosion pitting distribution parameters had little effect on the final fatigue life. This was most likely due to the relatively little difference a few micrometres make when the pitted area is as small as it is and the stress gradient is quite high. Critical crack state and the crack growth curve have a larger impact on the final fatigue life and therefore introduces some uncertainty about the results. The best results however, are based on the most optimistic parameters being correct. Abaqus stress results most likely have a large impact on the final fatigue life, and this introduces a very challenging situation, to properly design a FEM model with the limited description of test conditions.

8. Conclusion

The purpose of this thesis has been to investigate the subject of corrosion pitting fatigue and its possible application to the LINKpfat RDA-module. Investigation into the interaction between corrosion pitting and fatigue was performed to enable the creation of a manual model that could be used to validate the RDA-module. Comparisons between the manual model and LINKpfat was carried out on simple components. Results appear consistent, but will of course need more calculation tests on a wider variety of geometries to be fully validated. Several issues were resolved during the work, but this is also of some concern because there can be several other problems that was not discovered with these tests.

Corrosion pitting data was an important part of the thesis assignment. Finding comprehensive studies with readily available input parameters that could fit a LINKpfat analysis proved difficult. The fatigue test data that was used was from the most detailed report that was found during the literature review. Even though the results gave relatively conservative results, they can be deemed good for such a quick investigation considering all the uncertainty related to several of the parameters. Generally, the fatigue results could be found within a reasonable range, with a few results varying greatly from the expected results. These outliers can have varying explanations, however finding the cause of this issue is recommended for further investigation to help understand why they have occurred. One suspected reason is the initial sorting of all the defects when the software decides which is the critical one. The first increment of crack growth that is calculated might not be the real critical defect for certain geometries and stress gradients. Strengths and weaknesses for this method should be given a further investigation to give even more credibility to the results.

Even though the results of this fatigue test generated reasonable results more test needs to be performed to thoroughly validate the software for application on corrosion pitting fatigue problems. Corrosion pitting can occur with varying geometry for each pit, and for some materials they may occur close together in clusters. LINKpfat cannot consider crack growth interaction and branching effects that may occur during some fatigue situations. Material and corrosion behaviour should be well known and specified before the LINKpfat approach can be taken for the given problem.

8.1 Recommendations for further work

More testing on materials with corrosion pits with initial aspect ratio close to 1 should be conducted. Being able to do fatigue tests with larger sample sizes and full control on both corrosive and load conditions could be of great benefit when validating the software for potential industrial application. It would be of interest to be able to determine statistically representative defect distributions along with proper 3D modelling of the stress condition, which the component may experience. Examination of the application of statistics of extremes, with the block-maxima and peak-over threshold method, could also be outlined to discover the most efficient method of characterizing a corrosion pit size distribution.

LINKpfat could be improved by including more extreme value distributions or allowing the user to define the distribution themselves. Improved options to visualize all generated defects and the critical ones could be designed and programmed. Now there is a slight visual bug that hides some or the generated defects when viewing from certain angles.

9. References

[1] B. R. Crawford, C. Loader, Q. Liu, T. J. Harrison and P. K. Sharp, "Can pitting corrosion change the location of fatigue failure in aircraft?," *International Journal of Fatigue - Volume 61,* pp. 304-314, April 2014.

[2] ASTM International, "Standard Terminology Relating to Fatigue and Fracture Testing E1823-13," ASTM International, 2013.

[3] N. E. Dowling, Mechanical Behavior of Materials, International 4th ed., Pearson Education, 2012.

[4] J. Schijve, Fatigue of Structures and Materials, 2nd Ed, Springer, 2008.

[5] K. Nisancioglu, Corrosion Basincs and Engineering, Lecture Notes, Trondheim: NTNU, 2014.

[6] W. Qiangyuan, N. Kawagoishi, Q. Chen and R. M. Pidaparti, "Evaluation of the probability distribution of pitting corrosion fatigue life in aircraft materials," *Acta Mechanica Sinica - Volume 19, No. 3,* 3 June 2003.

[7] R. Mathis, "Initiation and early growth mechanisms of corrosion fatigue cracks in stainless steels," *Journal of Materials Science 22,* pp. 907-914, 1987.

[8] I. Milne, R. O. Ritchie and L. Karihaloo, Comprehensive Structural Integrity: Cyclic loading and fatigue, Elsevier, 2003.

[9] D. W. Hoeppner, V. Chandrasekaran and A. M. H. Taylor, "Review of pitting corrosion fatigue models, ICAF'99," 1999.

[10] Q. Y. Wang, R. M. Pidaparti and M. J. Palakal, "Comparative study of corrosion - fatigue in aircraft materials," *AIAA Journal - Vol. 39, No. 2,* pp. 325-330, February 2001.

[11] J. J. Medved, M. Breton and P. E. Irving, “Corrosion pit size distributions and fatigue lives - a study of the EIFS technique for fatigue design in the presence of corrosion,” *International Journal Fatigue 26,* pp. 71-80, 2004.

[12] K. K. Sankara, R. Perez and K. V. Jata, “Effects of pitting corrosion on the fatigue behavior of aluminum alloy 7075-T6: modeling and experimental studies,” *Materials Science and Engineering A297,* pp. 223-229, 2001.

[13] M. Jasiczek, J. Kaczorowski, E. Kosieniak and M. Innocenti, “A New Approach to Characterization of Gas Turbine Components Affected by Pitting Corrosion,” *Journal of Failure Analysis and Prevention Volume 12,* pp. 305-313, June 2012.

[14] S. Dey, M. K. Gunjan and I. Chattoraj, “Effect of temper on the distribution of pits in AA7075 alloys,” *Corrosion Science 50,* pp. 2895-2901, 2008.

[15] J. Grum and U. Zupanc, “Effect of pitting corrosion on fatigue performance of shot-peened aluminium,” *Journal of Materials Processing Technology 210,* pp. 1197-1202, 2010.

[16] A. Wormsen, A. Fjeldstad and G. Härkegård, “A post-processor for fatigue crack growth analysis based on a finite element stress field,” *Computer Methods for Applied Mechanical Engineering - Volume 197,* pp. 834-845, 5 Januar 2008.

[17] Sintef Materialer og Kjemi, Trondheim, “LINKpfat 1.2.0.14 User Manual,” SINTEF.

[18] T. Mills, P. K. Sharp and C. Loader, “The Incorporation of Pitting Corrosion Damage into F-111 Fatigue Life Modelling, DSTO-RR-0237,” DSTO Aeronautical and Maritime Reseach Laboratory, 2002.

[19] X.-Y. Zhang, S.-X. Li, R. Liang and R. Akid, “Effect of corrosion pits on fatigue life and crack initiation,” in *13th International Conference on Fracture*, Beijing, 2013.

[20] N. Acuña, J. González-Sánchez, G. Kú-Basulto and L. Domínguez, “Analysis of the stress intensity factor around corrosion pits developed on structures subjected to mixed loading,” *Scripta Materialia 55,* pp. 363-366, 2006.

[21] J. E. Zamber and B. M. Hillberry, “Probabilistic Approach to Predicting Fatigue Lives of Corroded 2024-T3,” *AIAA Journal Vol. 37,* 10 October 1999.

[22] S.-X. Li and R. Akid, “Corrosion fatigue life prediction of a steel shaft material in seawater,” *Engineering Failure Analysis 34,* pp. 324-334, 2013.

[23] G. Härkegård, “Short-crack modelling of the effect of corrosion pits on the fatigue limit of a 12% Cr steel (extended abstract),” 2nd International Symposium on Fatigue Design & Material Defects., Paris, 13-14 June 2014.

[24] X.-G. Huang and J.-Q. Xu, “3D analysis for pit evolution and pit-to-crack transition during corrosion fatigue,” *Journal of Zhejiang University - Science A (Applied Physics & Engineering),* pp. 292-299, 2013.

[25] B. R. Crawford, C. Loader, T. J. Harrison and Q. Liu, “A demonstration using low-kt fatigue specimens of a method for predicting the fatigue behaviour of corroded aircraft components,” Austrailia Air Vehicles Division DSTO-RR-0390, Melbourne, 2013.

[26] B. Schönbauer, S. Stanzl-Tschegg, N. Rieger, R. Salzman and R. Gandy, “Influence of Corrosion Pits on the Fatigue Limit of 12% Cr Steam Turbine Blade Steel,” ICF13, 2013.

[27] C. W. Anderson, J. de Maré and R. H., “Methods for estimating the sizes of large inclusions in clean steels,” *Acta Materialia - Vol 53,* pp. 2295-2304, 23 February 2005.

[28] E. R. Dougherty, Probability and statistics for the engineering, computing and physical sciences, Prentice-Hall International, Inc, 1990.

[29] P. K. Sharp, T. Mills and G. Clark, “Aircraft Structural Integrity: The Impact of Corrosion,” Defence Science and Technology Organisation.

[30] B. R. Crawford, T. J. Harrison, C. Loader, Q. L. H. G. Liu and P. K. Sharp, “The Combined Effect of Stress Concentrators and Pitting Corrosion on the Location of Fatigue Failures in Aircraft Components,” DSTO, 2014.

[31] B. Dodson, The Wibull Analysis Handbook, 2nd ed., Milwaukee: Quality Press, 2006.

[32] Mathwave Technologies, “Mathwave - data analysis & simulation,” [Online]. Available: http://www.mathwave.com/en/home.html. [Accessed 5 April 2015].

[33] Matchwave Technologies, “EasyFit 5.6 -Example distributions,” 2015.

[34] S. Coles, An Introduction to Statistical Modeling of Extreme Values, London: Springer-Verlag, 2001.

[35] Mann and T, “The influence of mean stress on fatigue crack propagation in aluminium alloys.,” *International Journal of Fatigue 29,* pp. 1393-1401, 26 January 2007.

[36] B. R. Crawford and P. Khan Sharp, “Equivalent Crack Size Modelling of Corrosion Pitting in an AA7075-T7451 Aluminium Alloy and its Implications for Aircraft Structural Integrity,” DSTO Defence Science and Technology Organisation, 2012.

[37] I. Løtveit and A. Rasten, “Validering av postprosessor for utmattingsvurdering av enkle komponent- og sprekkgeometrier,” Master thesis NTNU, Trondheim, 2014.

[38] P. P. Milella, Fatigue and Corrosion in Metals, Springer, 2012.

[39] M. Shirani and G. Härkegård, “Damage tolerant design of cast components based on defects detected by 3D X-ray computed tomography,” *International Journal of Fatigue - Vol 41,* pp. 188-198, 18 October 2012.

[40] P. Shi and S. Mahadevan, “Damage tolerance approach for probabilistic pitting corrosion fatigue life prediction,” *Enginering Fracture Mechanichs - Vol. 68,* pp. 1493-1507, 5 October 2001.

[41] B. R. Crawford, T. J. Harrison, C. Loader, Q. Liu, G. Härkegård and P. K. Sharp, “The Combined Effect of Stress Concentrators and Pitting Corrosion on the Location of Fatigue Failures in Aircraft Components,” DSTO, Australia, 2014.

[42] A. W. Peabody, Control of Pipeline Corrosion, Second Edition, NACE International, 2001.

Appendix A.1 – Probability distributions

Normal distribution

$$f(x,\mu,\sigma) = \frac{1}{\sqrt{2\pi\sigma^2}} e^{-\frac{(x-\mu)^2}{2\sigma^2}} \tag{15}$$

$$F(x,\mu,\sigma) = \frac{1}{2}\left[1 + erf\,\frac{(x-\mu)}{\sigma\sqrt{2}}\right] \tag{16}$$

Lognormal distribution

$$f(x,\mu,\sigma) = \frac{1}{x\sqrt{2\pi\sigma^2}} e^{-\frac{(ln\,x-\mu)^2}{2\sigma^2}} \quad x > 0 \tag{17}$$

$$F(x,\mu,\sigma) = \frac{1}{2}\left[1 + erf\,\frac{(ln\,x-\mu)}{\sigma\sqrt{2}}\right] \tag{18}$$

Appendix A.2 – Other calculation equations

Arc length

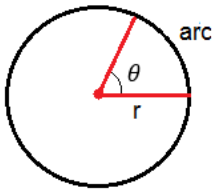

$$arc\ length = \theta * \frac{\pi}{180} r \tag{19}$$

Arithmetic mean (average)

$$\overline{X} = \frac{1}{2}\sum_{i=n}^{n} x_i \tag{20}$$

$$Range = maximum - minimum \tag{21}$$

$$Percent\ relative\ range\ (PRR) = \frac{Range}{Average} * 100 \tag{22}$$

Uncorrected sample standard deviation.

$$s = \sqrt{\frac{1}{N}\sum_{i=n}^{n}(X_i - \overline{X})^2} \tag{23}$$

Appendix A.3 – Weibull regression line

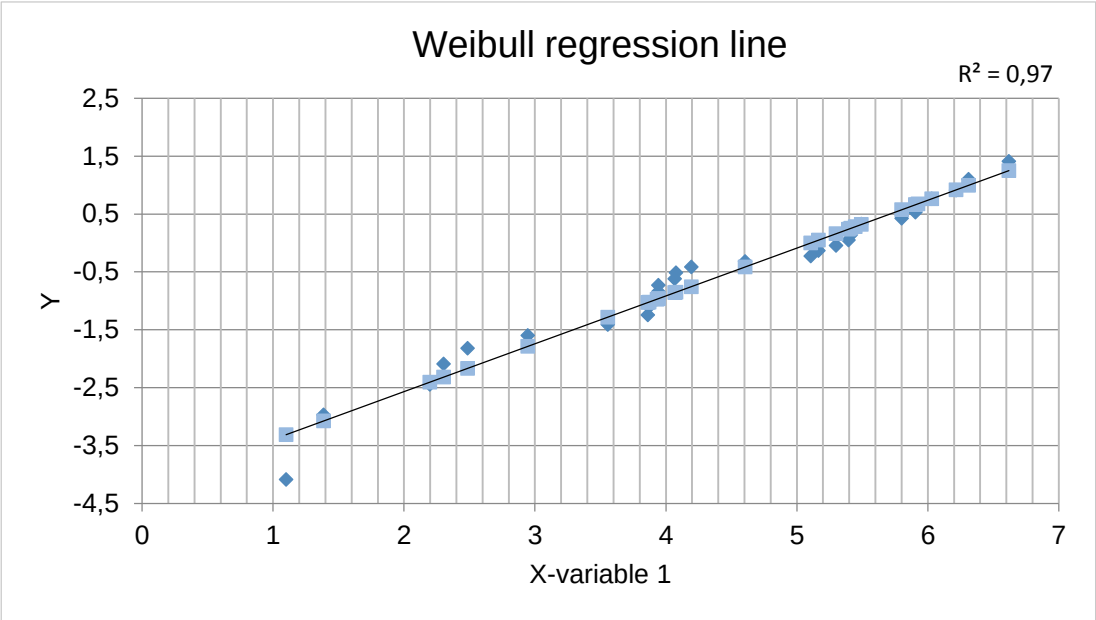

Figure 35: Excel regression of Weibull fit with R-squared value.

Appendix B.1 – Case 1, simplified turbine blade in tension

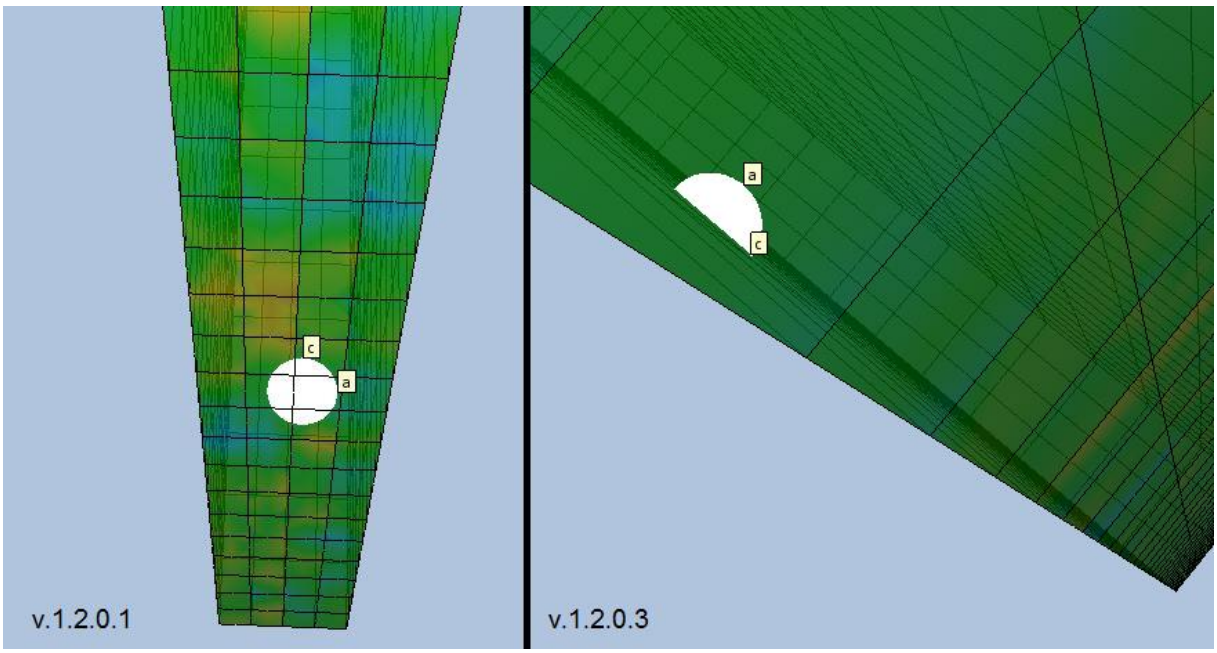

Figure 36: LINKpfat v.1.2.0.1 (on the left) defined the input of surface crack as an embedded crack in some cases. The picture on the right shows the correctly oriented surface crack from v.1.2.0.3 and above with the same input parameters.

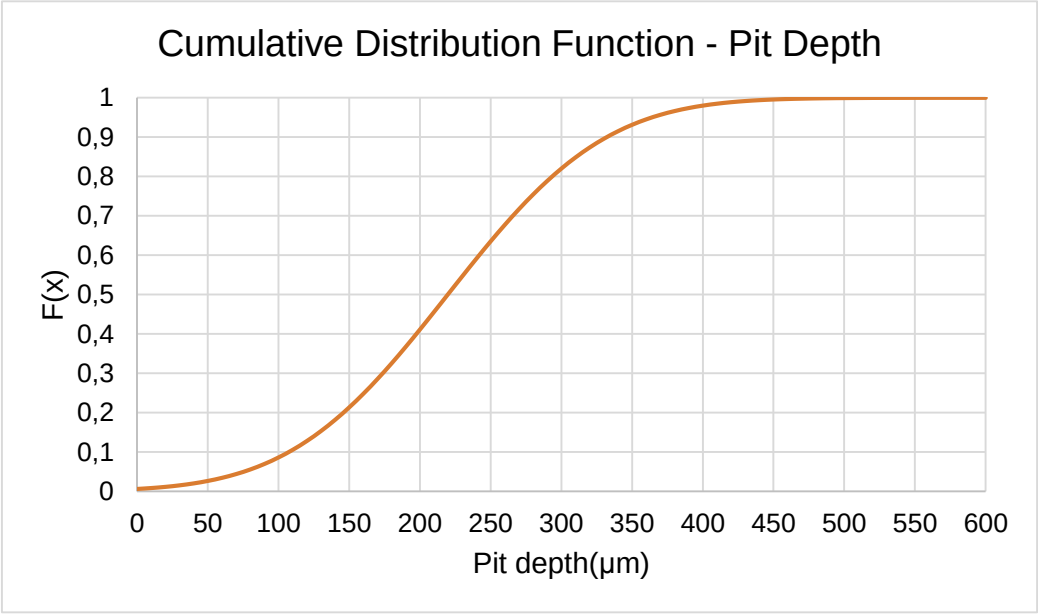

Figure 37: Cumulative distribution function for the normal curve with σ = 219.63 µm and μ = 87.678 µm.

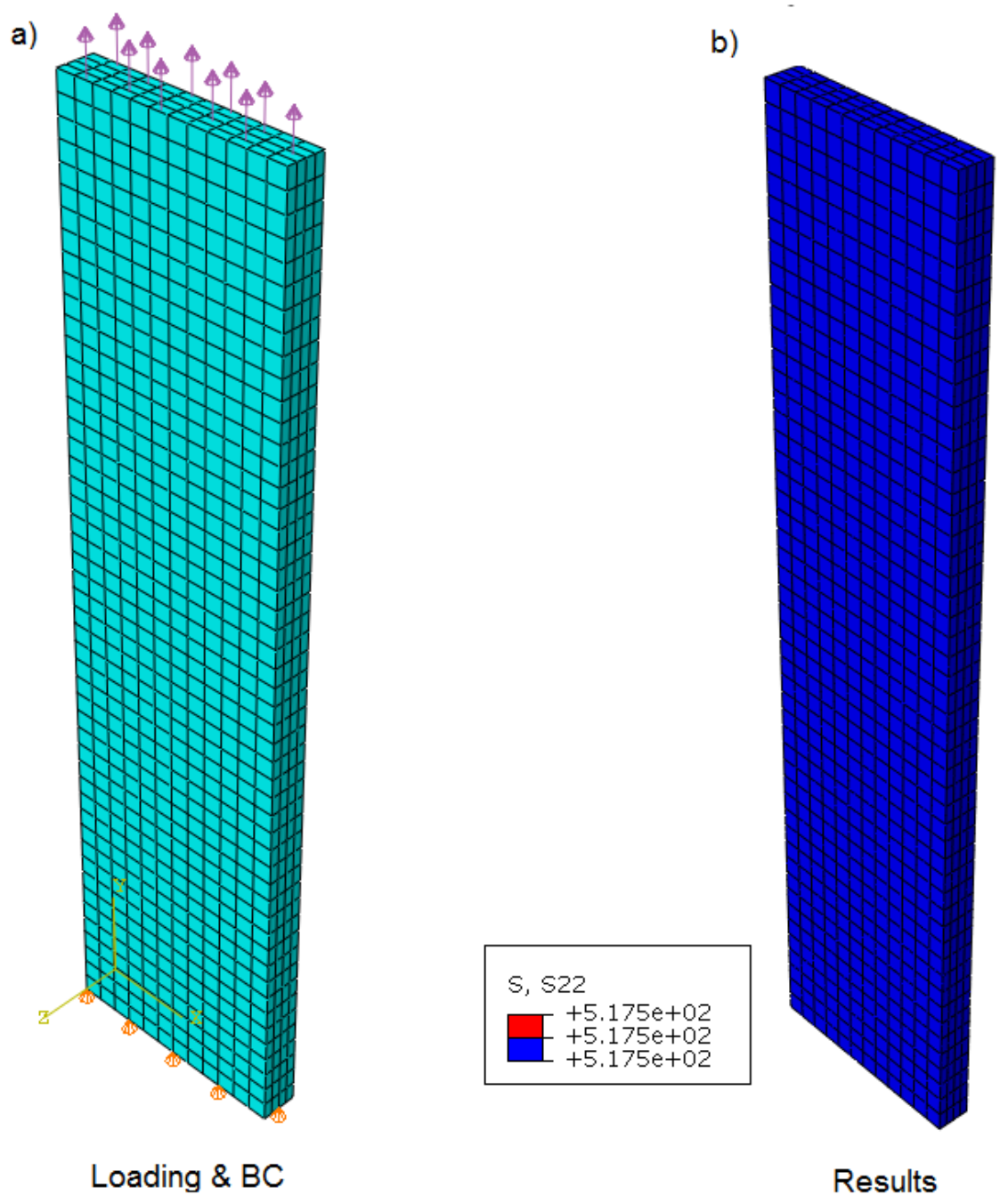

Figure 38: a) Loading with uniform stress on top surface. Boundary conditions at bottom part ensures no stress concentrations due to locking. b) Results from show uniform mean stress loading direction (y/22) direction. Amplitude in LINKpfat modeled as $1/9^{th}$ of the mean stress.

Appendix B.2 – Case 2, simplified turbine blade in bending

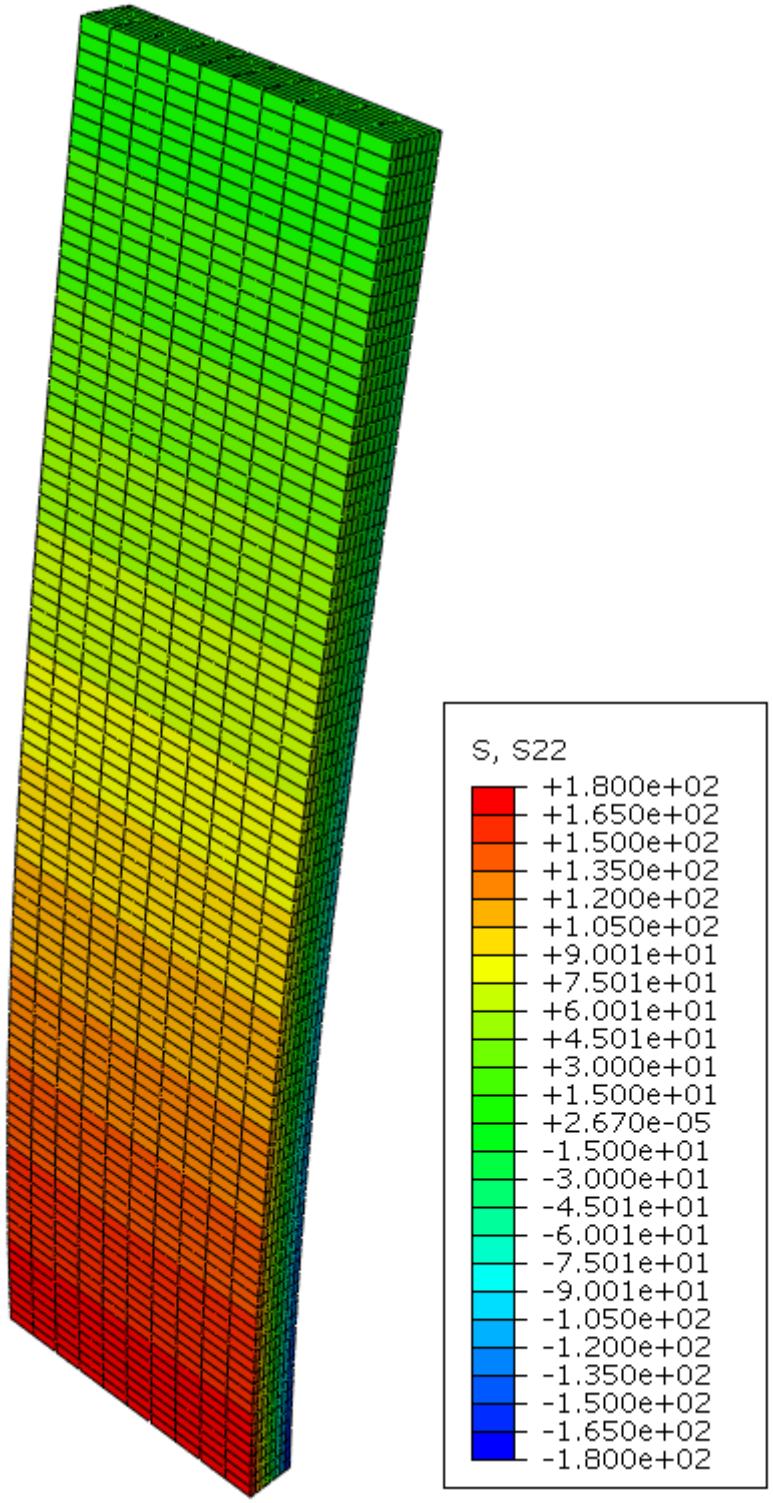

Figure 39: Abaqus model showing the tension stress on front side of the component that will be attacked by corrosion pitting.

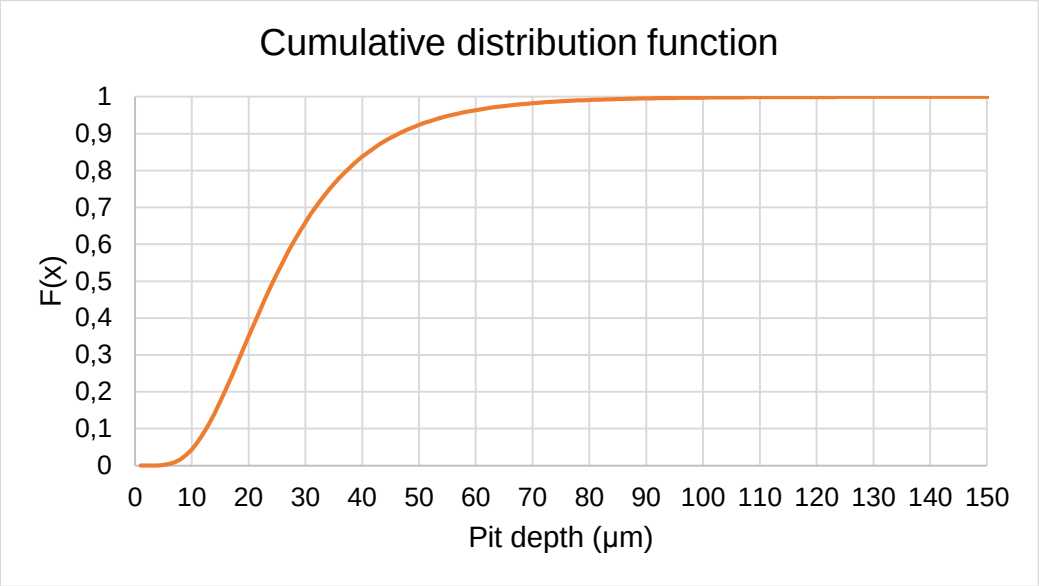

Figure 40: CDF for the lognormal distribution used in manual calculations.

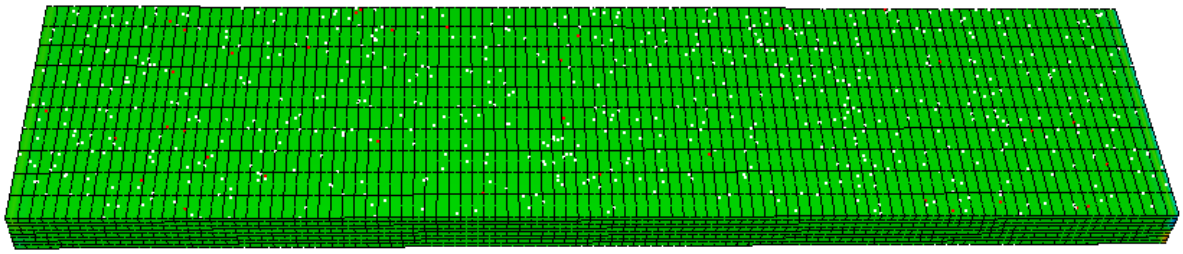

Figure 41: All initial defects generated on component #3 in Case 2a.

Table 25: Fatigue life and critical defect size for each section calculated for component #1.

Location	**Crit. def. a_i [µm]**	**N_f [cycles]**
1	69	$3{,}60 * 10^{11}$
2	69	$8{,}87 * 10^{9}$
3	75	$1{,}46 * 10^{9}$
4	48	$7{,}25 * 10^{8}$
5	75	$2{,}01 * 10^{8}$
6	65	$1{,}18 * 10^{8}$
7	76	$5{,}74 * 10^{7}$
8	114	$2{,}26 * 10^{7}$
9	44	$3{,}95 * 10^{7}$
10	66	$1{,}84 * 10^{7}$
11	76	$1{,}14 * 10^{7}$
12	63	$1{,}01 * 10^{7}$
13	48	$9{,}93 * 10^{6}$
14	78	$4{,}76 * 10^{6}$
15	67	$4{,}37 * 10^{6}$
16	48	$4{,}81 * 10^{6}$
17	47	$3{,}97 * 10^{6}$
18	79	$1{,}96 * 10^{6}$
19	93	$1{,}36 * 10^{6}$
20	54	$1{,}99 * 10^{6}$
21	**119**	**$7{,}24 * 10^{5}$**
22	84	$9{,}17 * 10^{5}$
23	69	$9{,}68 * 10^{5}$
24	66	$8{,}72 * 10^{5}$

Appendix C.1 – Case 3 calculation input

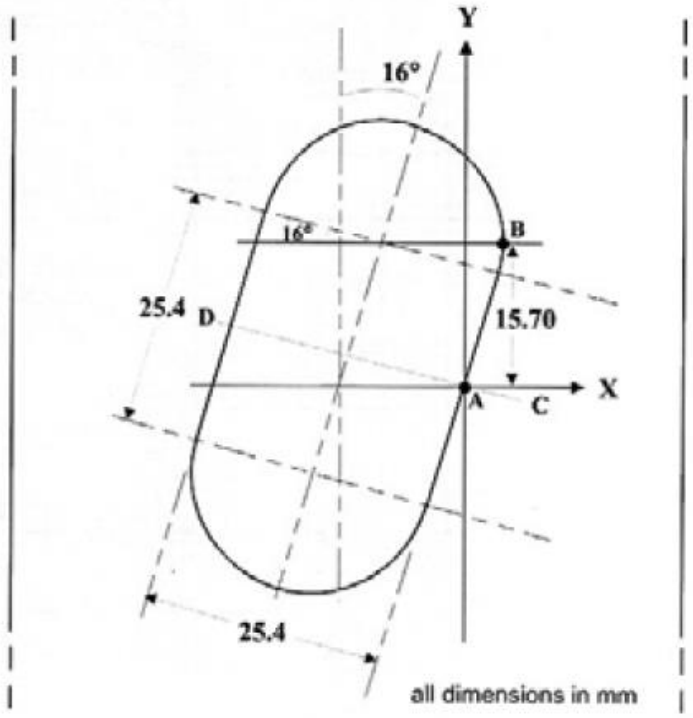

Figure 42: Detail of the hole in the specimen Figure 25 [18].

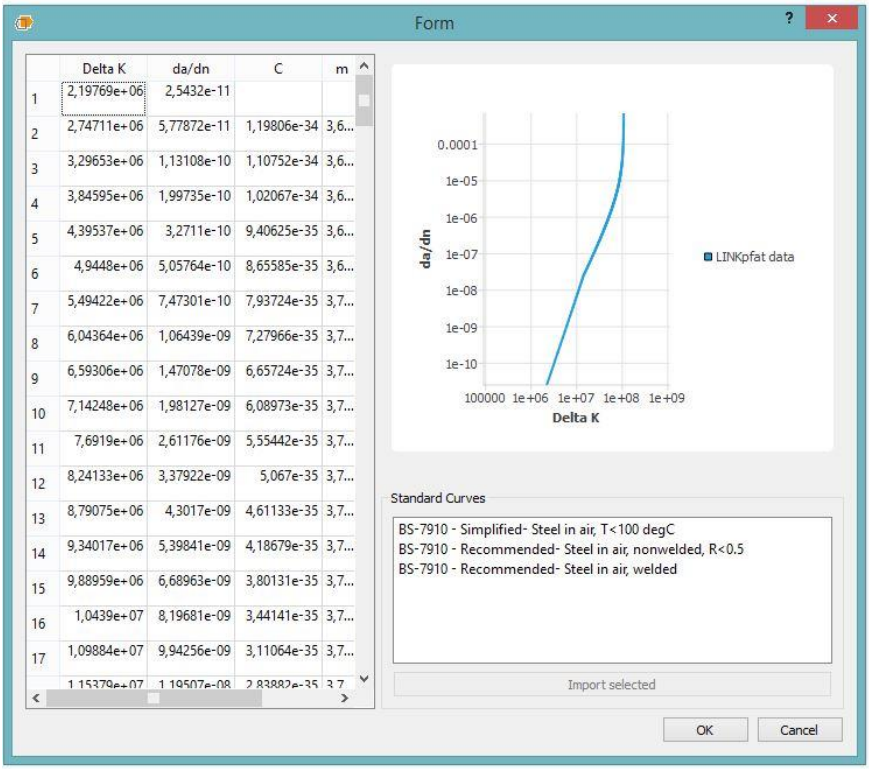

Figure 43: Forman data points applied to LINKpfat Paris curve approximation.

Appendix C.2 – Case 3 calculation results extra

Main Calculation results

Forman fit

Table 26: Number of pits generated for the Forman-fit calculations in Table 17.

Peak stress [MPa]	**896**	**1144**	**1310**	**1386**
Max number of pits	73	77	73	78
Min number of pits	41	42	43	36
Average number of pits	57,1	58,0	57,4	56,5
Standard deviation	7,3	7,8	7,3	7,7

LMTAS Mean fit

Table 27: Critical pit depths generated for the LMTAS Mean fit calculations in Table 19

Peak stress [MPa]	**896**	**1144**	**1310**	**1386**
Max crit. pit depth [μm]	145	138	137	183
Min crit. pit depth [μm]	63	62	71	64
Average crit. pit depth [μm]	93	87	95	95
Standard deviation	17	16	15	17

Table 28: Number of pits generated on LMTAS Mean fit calculations in Table 19.

Peak stress [MPa]	**896**	**1144**	**1310**	**1386**
Max number of pits	78	79	71	79
Min number of pits	36	41	43	39
Average number of pits	57,5	57,5	57,1	58,9
Standard deviation	8,1	7,2	6,6	8,2

Max pit depth

Table 29: Number of pits drawn during maximum pit size testing.

Stress level [MPa]		**896 MPa**			**1310 MPa**	
Max pit depth [µm]	95	120	∞	95	120	∞
Max number of pits	79	79	73	79	77	73
Min number of pits	42	44	41	41	35	43
Average number of pits	57,7	57,9	57,0	58,7	58,3	57,4
Standard deviation	7,3	6,7	7,3	7,6	7,9	7,3

Pit density

Table 30: Critical pit sizes from pit density testing.

Stress level [MPa]		**896 MPa**			**1310 MPa**	
Max pit depth [µm]	95	120	∞	95	120	∞
Max. pit depth [µm]	94	95	94	94	95	94
Min. pit depth [µm]	63	68	72	60	68	64
Avg. pit depth [µm]	80	86	84	79	89	84
Standard deviation	8,5	5,9	5,7	8,2	6,0	7,1

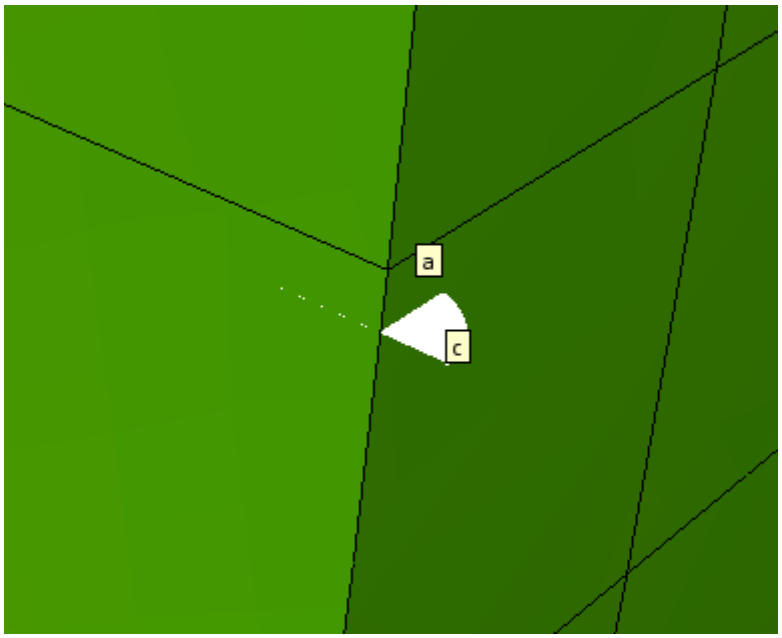

Figure 44: Initial crack located at edge of component for the defect resulting in a fatigue life of 33263.

Critical crack state

Table 31: Pit sizes drawn during critical crack state testing.

Stress level [MPa]	**896 MPa**			**1310 MPa**		
K_{Ic} [MPa√m]	46,5	60,35	74,1	46,5	60,35	74,1
Max. pit depth [µm]	95	95	94	95	94	94
Min. pit depth [µm]	60	65	72	67	65	64
Avg. pit depth [µm]	85	84	84	84	84	83
Standard deviation	5,9	7,3	5,8	6,3	6,5	7,1

Table 32: Number of pits drawn during critical crack state testing.

Stress level [MPa]	**896 MPa**			**1310 MPa**		
K_{Ic} [MPa√m]	46,5	60,35	74,1	46,5	60,35	74,1
Max number of pits	75	76	79	80	85	79
Min number of pits	43	39	42	40	38	41
Avg. number of pits	57,8	56,6	57,7	57,8	58,1	58,7
Standard deviation	6,1	8,2	7,7	7,6	7,8	7,6